Phytomedicine 132 (2024) 155806

Contents lists available at ScienceDirect

Phytomedicine

journal homepage: www.elsevier.com/locate/phymed

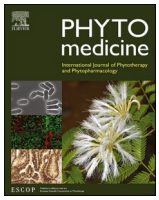

Original Article

Jingangteng capsules ameliorate liver lipid disorders in diabetic rats by regulating microflora imbalances, metabolic disorders, and farnesoid X receptor

Mi Chen [a,1], Manjun Gao [a,1], Hao Wang [b], Qingjie Chen [a], Xiufen Liu [a], Qigui Mo [a], Xingqiong Huang [a], Xiaochuan Ye [b,*], Dandan Zhang [a,*]

[a] Hubei Key Laboratory of Diabetes and Angiopathy, Hubei University of Science and Technology, No. 88 Xianning Avenue, Xian'an District, Xianning, Hubei Province 437100, PR China

[b] Hubei Key Laboratory of Resources and Chemistry of Chinese Medicine, Hubei University of Chinese Medicine, No. 16 West Huangjiahu Road, Hongshan District, Wuhan, Hubei Province 430065, PR China

ARTICLE INFO

Keywords:
Jingangteng capsules
Liver lipid disorders
Diabetic rats
Intestinal microbiota
Farnesoid X receptor (FXR)
Metabolomics

ABSTRACT

Background: The plant *Smilax china* L., also known as Jingangteng, is suspected of regulating glucose and lipid metabolism. Jingangteng capsules (JGTCs) are commonly used to treat gynecological inflammation in clinical practice. However, it is not clear whether JGTCs can regulate glucose and lipid metabolism, and the mechanism is unclear.

Purpose: To investigate the impact and mechanism of action of JGTCs on diabetes and liver lipid disorders in rats.

Methods: The chemical constituents of JGTCs were examined using ultra-high-performance liquid chromatography with quadrupole time-of-flight mass spectrometry. A high-fat diet and streptozotocin-induced diabetes model was used to evaluate anti-diabetic effects by assessing blood glucose and lipid levels and liver function. The mechanism was explored using fecal 16S rRNA gene sequencing and metabolomics profiling, reverse transcription-quantiative polymerase chain reaction (RT-qPCR), and Western blot analysis.

Results: Thirty-three components were identified in JGTCs. The serological and histomorphological assays revealed that JGTC treatment reduced levels of blood glucose and lipids, aspartate aminotransferase, alanine aminotransferase, and lipid accumulation in the liver of diabetic rats. According to 16S rDNA sequencing, JGTCs improved species richness and diversity in diabetic rats' intestinal flora and restored 22 dysregulated bacteria to control levels. Fecal metabolomics analysis showed that the altered fecal metabolites were rich in metabolites, such as histidine, taurine, low taurine, tryptophan, glycerophospholipid, and arginine. Serum metabolomics analysis indicated that serum metabolites were enriched in the metabolism of glycerophospholipids, fructose and mannose, galactose, linoleic acid, sphingolipids, histidine, valine, leucine and isoleucine biosynthesis, and tryptophan metabolism. Heatmaps revealed a strong correlation between metabolic parameters and gut microbial phylotypes. Molecular biology assays showed that JGTC treatment reversed the decreased expression of farnesoid X receptor (FXR) in the liver of diabetic rats and inhibited the expression of lipogenic genes (*Srebp1c* and *FAS*) as well as inflammation-related genes (interleukin (*IL)-β*, tumor necrosis factor (*TNF)-α*, and *IL-6*). Liver metabolomics analysis indicated that JGTC could significantly regulate a significant number of bile acid metabolites associated with FXR, such as glyco-beta-muricholic acid, glycocholic acid, tauro-beta-muricholic acid, and tauro-gamma-muricholic acid.

Abbreviations: ALT, alanine aminotransferase; AUC, area under the curve; AST, aspartate aminotransferase; DM, diabetes mellitus; FBG, fasting blood glucose; FXR, farnesoid X receptor; HFD, high-fat diet; H&E, hematoxylin and eosin; JGTCs, jingangteng capsules; JGTC-L, low-dose JGTC treatment; JGTC-H, high-dose JGTC treatment; LDA, linear discriminant analysis; LDL-C, low-density lipoprotein; LEfSe, linear discriminant analysis effect size; OGTT, oral glucose tolerance test; OPLS-DA, orthogonal partial least squares-discriminant analysis; PCA, principal component analysis; RT-qPCR, reverse transcription-quantitative polymerase chain reaction; SC, *Smilax china* L.; STZ, streptozotocin; TCM, traditional Chinese medicine; TC, total cholesterol; TG, triglycerides; UHPLC-Q-Orbitrap MS, ultrahigh-performance liquid chromatography quadrupole-orbitrap tandem mass spectrometry; UPLC-QTOF-MS/MS, ultra-high-performance liquid chromatography with quadrupole time-of-flight mass spectrometry; VIP, variable importance in the projection.

* Corresponding authors.
E-mail addresses: chuan9069@hbtcm.edu.cn (X. Ye), Dandan8991@hbust.edu.cn (D. Zhang).

[1] These authors contributed equally to this work and should be considered as co-first authors.

https://doi.org/10.1016/j.phymed.2024.155806
Received 5 November 2023; Received in revised form 30 May 2024; Accepted 3 June 2024
Available online 4 June 2024

Conclusions: This was the first study to investigate the mechanisms of JGTCs' effects on liver lipid disorders in diabetic rats. JGTCs inhibited liver lipid accumulation and inflammatory responses in diabetic rats by affecting intestinal flora and metabolic disorders and regulating FXR-fat synthesis-related pathways to alleviate diabetic lipid disorders.

Introduction

Diabetes mellitus (DM) poses a significant global health concern, with a predicted incidence of approximately 147.2 million people by 2045 (Baothman et al., 2016). The complications of diabetes include liver lipopathy, cardiocerebrovascular disease, kidney disease, and neuropathy. An earlier study found that the disruption of lipid metabolism in the liver also serves as a significant contributing factor leading to the higher occurrence of complications like atherosclerosis, as well as cardiovascular and cerebrovascular diseases (Newman et al., 2012). Although many lipid-modifying drugs, including statins, fibrates, and nicotinic acid combined with hypoglycemic drugs, are used to treat diabetic lipid metabolism disorders, long-term treatment with Western medicine is associated with adverse reactions, such as headache, insomnia, depression, dyspepsia, and nausea (Kern et al., 2016; Garibotto et al., 2017). Traditional Chinese medicine (TCM) addresses both symptoms and causes, resulting in minimal side effects while comprehensively regulating the body. Therefore, TCM and natural medicine research are focused on the identification of hypoglycemic and lipid-lowering drugs with safe, definite curative effects and few side effects.

The dried rhizome of the Liliaceae plant *Smilax china* L. (SC) is also known as Jingangteng. In modern studies, SC has been shown to regulate lipid disorders in metabolic diseases (Yang et al., 2019). In obese mice, SC can reduce the levels of total cholesterol (TC) and triglycerides (TG), while enhancing the abundance and diversity of intestinal flora (Li et al., 2021). In addition, previous studies showed that SC inhibited α-glucosidase (Gan et al., 2016), decreased blood glucose concentrations, and increased the liver glycogen content in mice with alloxan-induced uracil disease (Ma et al., 1998). Jingangteng capsules (JGTCs) are a marketed drug prepared by the water extraction and alcohol precipitation of *Smilax china*. Clinically, JGTCs are used to treat gynecological inflammation and have an annual sales revenue of over 100 million yuan. However, the potential of JGTCs to regulate disordered hepatic lipid metabolism in individuals with DM has not yet been explored.

Diabetic liver lipid metabolism disorder refers to high levels of TC, TG, and low-density lipoprotein (LDL-C) in the blood of diabetic patients, leading to the deposition of large amounts of lipids in the liver, the fatty degeneration of hepatocytes and the formation of fatty liver. Recent studies identified intestinal dysbiosis and its metabolites as important factors in the development of hepatic lipid metabolism disorders in diabetes mellitus patients (Liu et al., 2020). Functional microbial metabolites produced by the gut microbiota have been shown to regulate insulin sensitivity and energy metabolism in rodent models of diabetes and in humans, and changes in metabolites, such as bile acids, fatty acids, and gut hormones, also led to elevated lipid levels and impaired insulin signaling (Heianza et al., 2019). The exchange of material and information between the gut microbiota and the host is crucial for the physiological function and metabolism of the host, with small molecule substances serving as the bridge. Changes in the intestinal microflora lead to corresponding alterations in the metabolism of substances to maintain a microecological balance between the intestinal flora and the host (Baothman et al., 2016; Hartstra et al., 2015). Multiomics analysis provides valuable information about biomarkers related to physiological and pathophysiological conditions (Huyiligeqi et al., 2016). Therefore, merging serum, liver, and fecal metabolomics data provides a more comprehensive metabolic profile.

The mechanism underlying the hypoglycemic and lipid-lowering effects of JGTCs on diabetic rats remains unclear. Therefore, we investigated the alterations in microbial species, as well as serum and fecal metabolomics, farnesoid X receptor (FXR) expression, and the inflammation-related signaling pathway, to reveal the mechanisms by which JGTCs exert their anti-diabetic and hypolipidemic effects. This information will provide a scientific basis for expanding the application of JGTCs in the clinic and the secondary development of JGTCs.

Materials and methods

Materials, chemicals, and reagents

JGTCs were purchased from FuRen Pharmaceutical Co., Ltd. (Tongcheng County, Xian'ning City, Hubei Province, China). Chengdu Pusi Biological Polytron Technologies Inc. (Chengdu, China) provided quercitrin (CAS: 522-12-3), chlorogenic acid (CAS: 327-97-9), engeletin (CAS: 572-31-6), and resveratrol (CAS: 501-36-0). Dapagliflozin (CAS: 461432-26-8) was obtained from Hanzun Bio-technology Co., Ltd. (Shanghai, China).

UPLC-QTOF-MS/MS analysis of JGTC sample solution

After removal from the capsules, the drug (10 mg) was dissolved in 5 mL of methanol and sonicated for 20 min. The supernatant was then collected and filtered (0.22 μm). The mobile phase consisted of 0.1 % formic acid water (solvent A) acetonitrile (solvent B). Gradient elution of the mobile phase was carried out 0–60 min (12–60 %B), 60–70 min (60–12 %B) with a flow rate of 0.4 mL/min. Mass spectrometry conditions are referred to previous study (Zhang et al., 2022a,b).

Animal treatments and biochemical assays

Male Wistar rats (180–220 g) were provided by the Hubei Beiente Biotechnology Co., Ltd (License SYXK(E) 2021-0027) Hubei, China). The experimental rats were maintained in a specific pathogen-free experimental animal room at the Hubei University of Science and Technology (License SYXK(E)2013-0071, Hubei, China) with free access to food and water. The Animal Experimental Ethics Committee of Hubei University of Science and Technology approved the study (2023-03-103).

After one week's acclimatization, 5 rats were randomly assigned to the control group, and the other rats were assigned to the diabetic group. A high-fat diet (HFD) (10 % lard, 5 % egg yolk powder, 15 % sucrose, 1 % cholesterol, and 0.2 % sodium cholate, purchased from Wuhan Chunyuhong Laboratory Animal Feed Co., Ltd.) was fed to the diabetic rats for 28 days. Streptozotocin (35 mg/kg) was then injected intraperitoneally into the rats. After one week, fasting blood glucose (FBG) levels were detected after fasting for 8 h. The model was considered to be successfully established in rats with an FBG level >11.1 mmol/l. These diabetic rats were divided into 4 groups based on FBG levels ($n = 6$): model, positive (dapagliflozin, 0.105 mg/kg), low-dose JGTC treatment (JGTC-L, 0.54 g/kg), and high-dose JGTC treatment (JGTC-H, equal to 1.62 g/kg). JGTCs and dapagliflozin tablets were suspended in pure water. An equal amount of pure water was administered intragastrically to both the control and model groups of rats. The dosing schedule lasted 4 weeks, after which oral glucose tolerance tests (OGTTs) were performed. Rats were fasted for 8 h before the administration of glucose (2.0 g/kg b.w.), and blood glucose levels were measured after 0, 30, 60, and 120 min using a Sannuo blood glucose meter (Sinocare Inc., China).

Table 1
Data from UPLC-QTOF/MS/MS on the major JGTC components in the negative mode.

Peak no.	Identification	RT [min]	Chemical formula	Neutral mass	Calculated $[M-H]^-$ (*m*/z)	Observed $[M-H]^-$ (*m*/z)	Error (ppm)	MS/MS
1	4-Hydroxybenzoic acid	5.90	$C_7H_6O_3$	138.0317	137.0239	137.0237	−1.46	92.9263, 109.0255
2	Caffeic acid	4.74	$C_9H_8O_4$	180.0423	179.0344	179.0343	−0.56	91.0585, 117.0359,135.0437
3	Resveratrol*	21.50	$C_{14}H_{12}O_3$	228.0786	227.0708	227.0702	−2.64	185.0294,164.0087
4	Oxyresveratrol	13.65	$C_{14}H_{12}O_4$	244.0736	243.0657	243.0642	−6.17	201.0120,173.9985,130.0413
5	trans-Piceatannol	12.66	$C_{14}H_{12}O_4$	244.0736	243.0657	243.0642	−6.17	174.0471,159.0431,129,9736
6	Naringenin	24.41	$C_{15}H_{12}O_5$	272.0685	271.0606	271.0629	8.49	187.0348,151.0098,107.0143
7	Kaempferol	29.63	$C_{15}H_{10}O_6$	286.0477	285.0399	285.0378	−7.37	218.0101,151.0023
8	Dihydrokaempferol	15.02	$C_{15}H_{12}O_6$	288.0634	287.0556	287.0569	4.53	259.0155,243.0259,201.0149
9	Eriodictyol	17.28	$C_{15}H_{12}O_6$	288.0634	287.051	287.05	−3.48	259.0221,243.0067,180.0028
10	(−)-catechin	3.10	$C_{15}H_{14}O_6$	290.079	289.0712	289.0727	5.19	245.0797,227.0640,205.0473,203.0698,135.0437,123.0438,109.0276
11	Quercetin	27.43	$C_{15}H_{10}O_7$	302.0427	301.0348	301.0315	−10.96	107.0121,121.0282,151.0023,
12	Taxifolin	12.78	$C_{15}H_{12}O_7$	304.0583	303.0505	303.0457	−15.84	285.0378,267.8192,241.0443
13	Gentianolic acid glycoside	1.76	$C_{14}H_{20}O_8$	316.1158	315.108	315.1054	−8.25	153.0170,180.0083,218.9878
14	Methyl gentianolic acid glycoside	3.81	$C_{14}H_{18}O_9$	330.0951	329.0873	329.0885	3.65	268.9901,191.0553,167.0331
15	3,5-Dihydroxy-4-methyl-3-O-glucoside	6.41	$C_{14}H_{18}O_9$	330.0951	329.0873	329.0847	−7.9	167.0331,191.0327,269.0471
16	Chlorogenic acid*	4.03	$C_{16}H_{18}O_9$	354.0951	353.0873	353.0847	−7.36	135.0437,179.0343,191.0553
17	Cryptochlorogenic acid	4.81	$C_{16}H_{18}O_9$	354.0951	353.0873	353.0847	−7.36	173.0436,179.0343,191.0553
18	Methyl chlorogenate	12.69	$C_{17}H_{20}O_9$	368.1107	367.1029	367.1003	−7.08	254.0564,178.9986,153.0170
19	(E/Z)-Polydatin	11.17	$C_{20}H_{22}O_8$	390.1315	389.1236	389.1218	−4.63	227.0671,242.0022
20	Unknown	21.57	$C_{21}H_{20}O_{10}$	432.1056	431.0978	431.0959	−4.41	285.0343,184.9932,320.0025
21	Engeletin*	23.36	$C_{21}H_{22}O_{10}$	434.1213	433.1135	433.1136	0.23	287.0543,269.0438,259.0538,180.0055,151.0023
22	Isoengeletin	20.76	$C_{21}H_{22}O_{10}$	434.1213	433.1135	433.1136	0.23	287.0534,269.0438,259.0583,180.0055,151.0023
23	Quercitrin*	22.27	$C_{21}H_{20}O_{11}$	448.1006	447.0927	447.0921	−1.34	301.0315,300.0268,271.0224,243.0291,151.0023
24	Cynaroside	20.10	$C_{21}H_{20}O_{11}$	448.1006	447.0927	447.0877	−11.18	285.0375,208.9332
25	Dihydrocaphen 3-O-β-D-glucoside	5.09	$C_{21}H_{22}O_{11}$	450.1162	449.1084	449.1034	−11.13	287.0534,259.0583,153.0170
26	Dihydrocaphen 5-O-β-D-glucoside	6.64	$C_{21}H_{22}O_{11}$	450.1162	449.1084	449.1077	−1.56	287.0534,269.0438,153.0170
27	Dihydrocaphen 7-O-β-D-glucoside	7.45	$C_{21}H_{22}O_{11}$	450.1162	449.1084	449.1077	−1.56	287.0534,269.0438,259.0583
28	Neoastilbin	14.58	$C_{21}H_{22}O_{11}$	450.1162	449.1084	449.1077	−1.56	303.0493,285.0378,178.9959,151.0375,125.0233
29	Astilbin	15.91	$C_{21}H_{22}O_{11}$	450.1162	449.1084	449.1077	−1.56	125.0233,151.0023,449.1034
30	Neoisoastilbin	19.29	$C_{21}H_{22}O_{11}$	450.1162	449.1084	449.1077	−1.56	303.0529,285.0378,178.9959,151.0375,125.0233
31	Isoastilbin#	20.22	$C_{21}H_{22}O_{11}$	450.1162	449.1084	449.1077	−1.56	303.0493,285.0378,178.9959,151.0375,125.0233
32	Taxifolin 3-O-glucoside	4.466	$C_{21}H_{22}O_{12}$	466.1111	465.1033	465.1004	−6.24	376.0091,303.0172,241.0093
33	Rutin	18.40	$C_{27}H_{30}O_{16}$	610.1534	609.1456	609.1483	4.43	300.0268,301.0315,229.1207,257.3998

* Compounds identified using reference compounds.
# Unrecognized isomer.

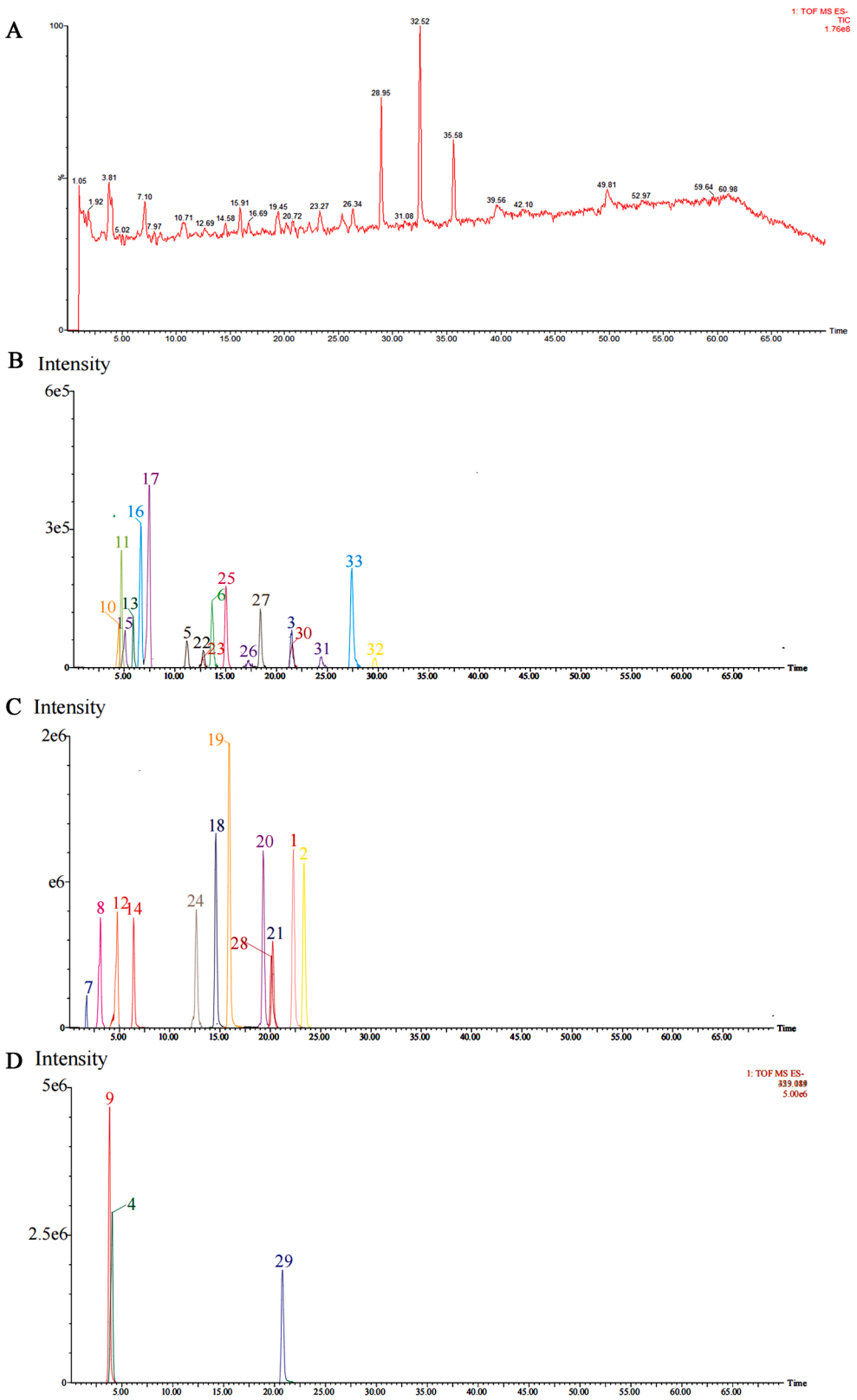

Fig. 1. Total ion chromatogram (A) and extracted ion chromatogram (B–D) of JGTCs based on UPLC-QTOF-MS/MS profiles in negative mode.

The proximity ladder-shaped formula was used to calculate the area under the curve (AUC) of blood glucose concentrations. On day 27 of the dosing phase, fecal samples were obtained from every rat. Rats were anesthetized with ether before euthanization by decapitation, and blood was then obtained from the abdominal aorta. The blood samples were centrifuged for 10 min at 1000 × *g* to obtain serum. Biochemical kits purchased from the Nanjing Jiancheng Bioengineering Institute (Nanjing, China) were used to measure the levels of the following serum markers: aspartate aminotransferase (AST) (CAT: C010-2-1, LOT: 202304024), alanine aminotransferase (ALT) (CAT: C009-2-1, LOT:

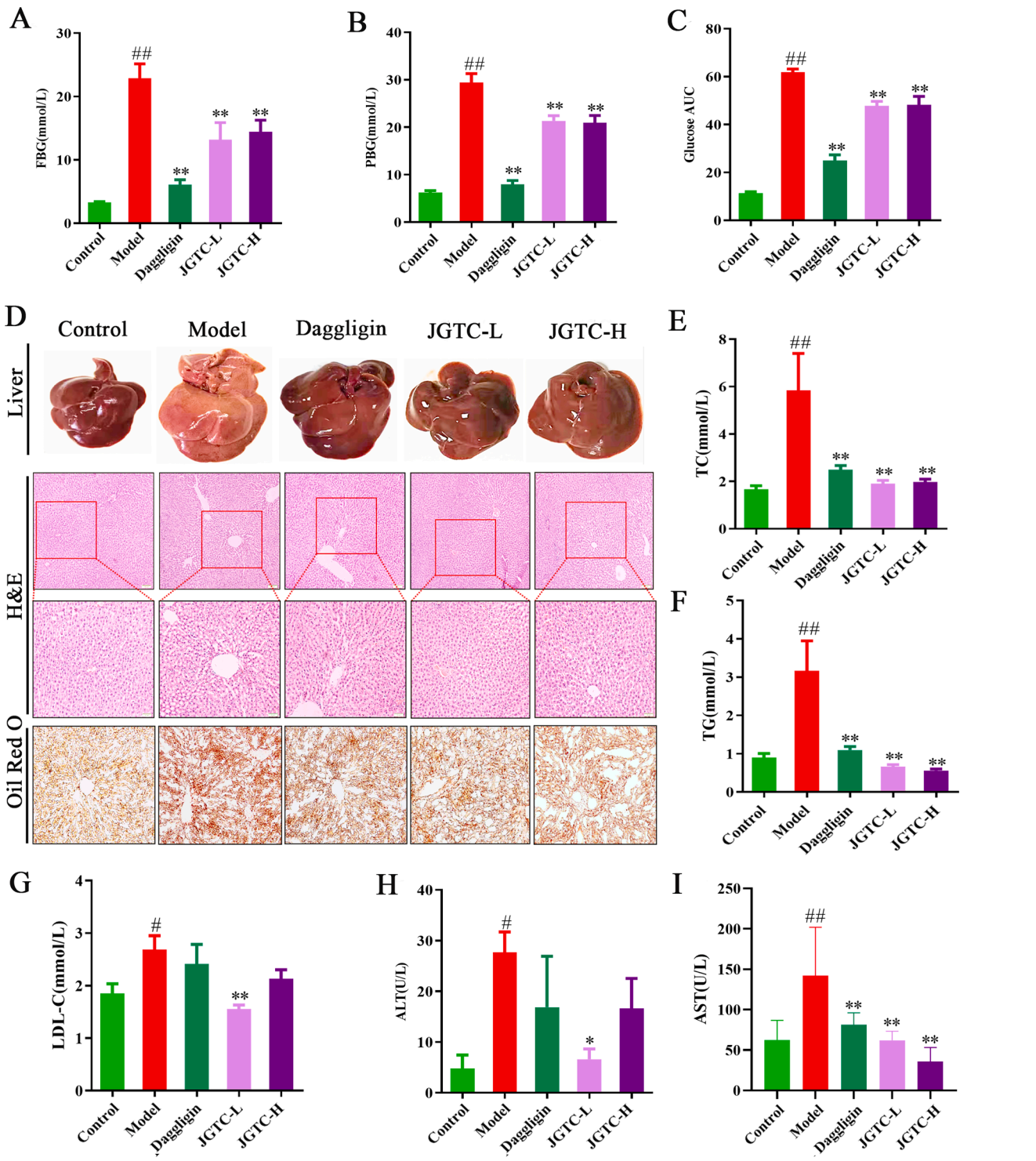

Fig. 2. JGTC regulates blood glucose and liver lipid accumulation in diabetic rats. (A–C) Biochemical indicators, including blood glucose levels. (D). Representative images of hematoxylin and eosin (H&E) and Oil Red O staining of rat liver. (E–G). TC (E), TG (F), and LDL-C (G) contents. (H and I) Liver function indexes ALT (H) and AST (I). JGTC-L, 0.54 g/kg treatment; JGTC-H, 1.62 g/kg treatment. $^{\#}P < 0.05$, $^{\#\#}P < 0.01$ vs. the control group; $^{*}P < 0.05$, $^{**}P < 0.01$ vs. the model group.

202304024), TC (CAT: A111-1-1, LOT: 202304024), TG (CAT: A110-1-1, LOT: 202304024), and low-density lipoprotein-cholesterol (LDL-C) (CAT: A113-1-1, LOT: 202304024).

For histological evaluation, livers were fixed in 4 % paraformaldehyde for 24 h, followed by routine dehydration and paraffin-embedding. For all subgroups, paraffin-embedded liver tissue was sectioned at 5 μm before hematoxylin and eosin (H&E) stainingto estimate the extent of liver lesions. Oil Red O staining was employed to identify lipid droplets in the liver tissues. These liver tissues were optimum cutting temperature compound (OCT)-embedded, sectioned at a thickness of 10 μm, and stained with the Modified Oil Red O Staining Kit (Beyotime, Shanghai, China) for 15 min.

Western blot analysis

Total proteins were extracted, and Western blots were performed

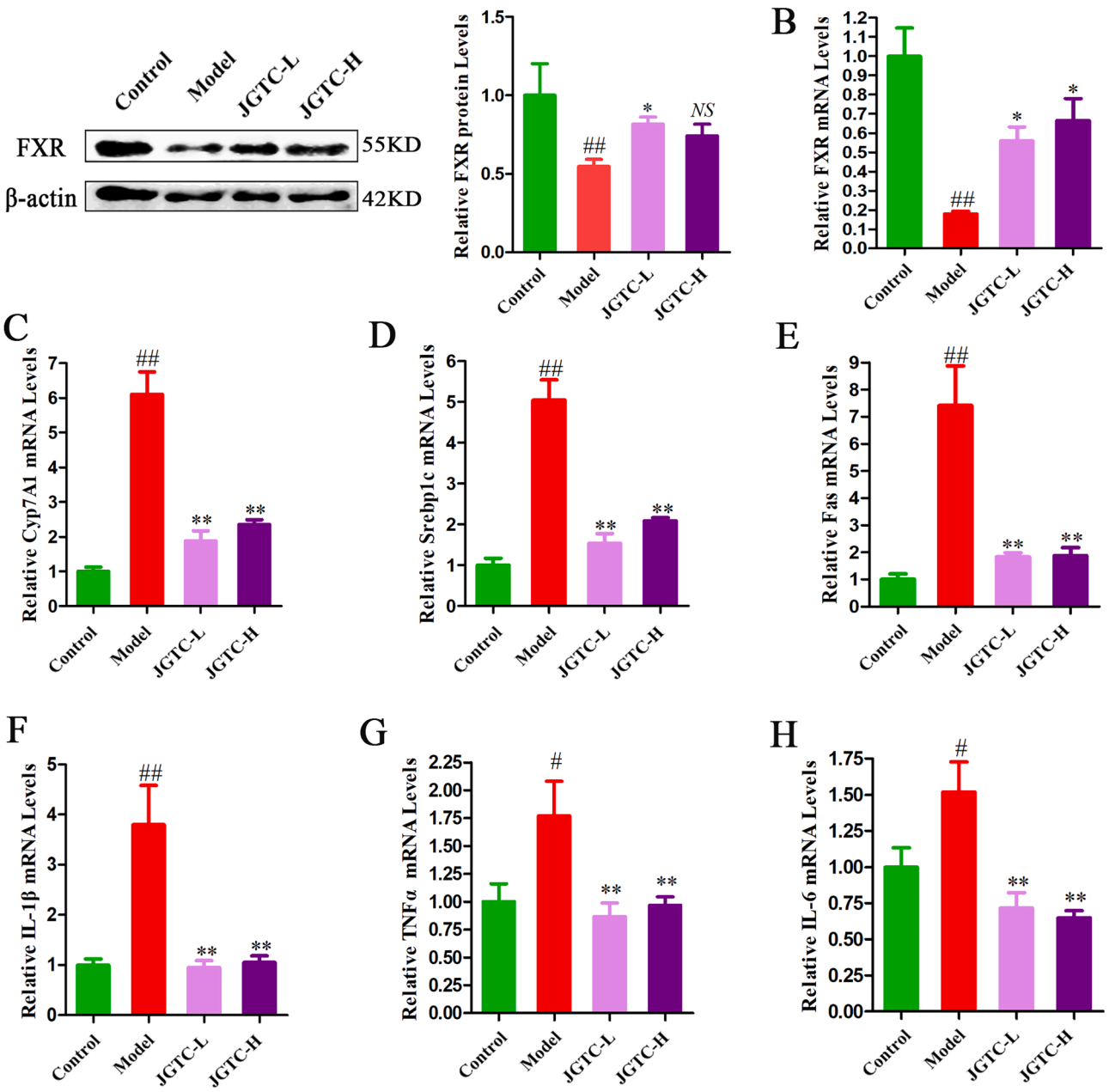

Fig. 3. JGTC regulates hepatic FXR and lipid metabolism-related gene expression in diabetic rats to alleviate liver injury. (A and B). Western blots and qRT-PCR analysis of the expression of FXR protein (A) and mRNA (B). (C-D). qRT-PCR analysis of the expression of lipid synthesis-related genes *CYP7A1* (C), *Srebp1c* (D), and *Fas* (E). (F-H). qRT-PCR analysis of the expression of inflammation-related genes *IL-1β* (F), *TNF-α* (G), and *IL-6* (H).

according to a previously described method (Chen et al., 2021) using antibodies to detect the following proteins: FXR (1:1000, sc-25309; Santa Cruz Biotechnology, Dallas, CA, USA) and β-actin (1:1000, sc-47778; Santa Cruz Biotechnology). Horseradish peroxidase-conjugated AffiniPure goat anti-mouse IgG (H + L) (1:5000, SA00001-1; Proteintech, Wuhan, China) was used as the secondary detection antibody, and the results were analyzed using ImageJ (National Institutes of Health, Bethesda, MD) software.

Quantitative real-time PCR

As described previously, RNA was extracted and reverse-transcribed to cDNA (Ding et al., 2020). Quantitative real-time polymerase chain reaction PCR (qRT-PCR) analysis was performed on the Bio-Rad CFX96 Real-Time PCR Detection System (Hercules, CA, USA) using the ChamQ SYBR qPCR Master Mix (Low ROX Premixed) (Vazyme, Nanjing, China), and the primers described in Supplementary Table 1. Data were normalized against β-actin, and relative gene expression was determined using the $2^{-\Delta\Delta CT}$ method.

16S rDNA gene sequencing analysis

16S rDNA sequencing of fecal samples collected from the rats and subsequent bioinformatics analysis was conducted using an Illumina NovaSeq 6000 platform to obtain 250-bp paired-end reads as previously described (Zhang et al., 2022a).

Metabolomics analysis

An extraction solution containing deuterated internal standards

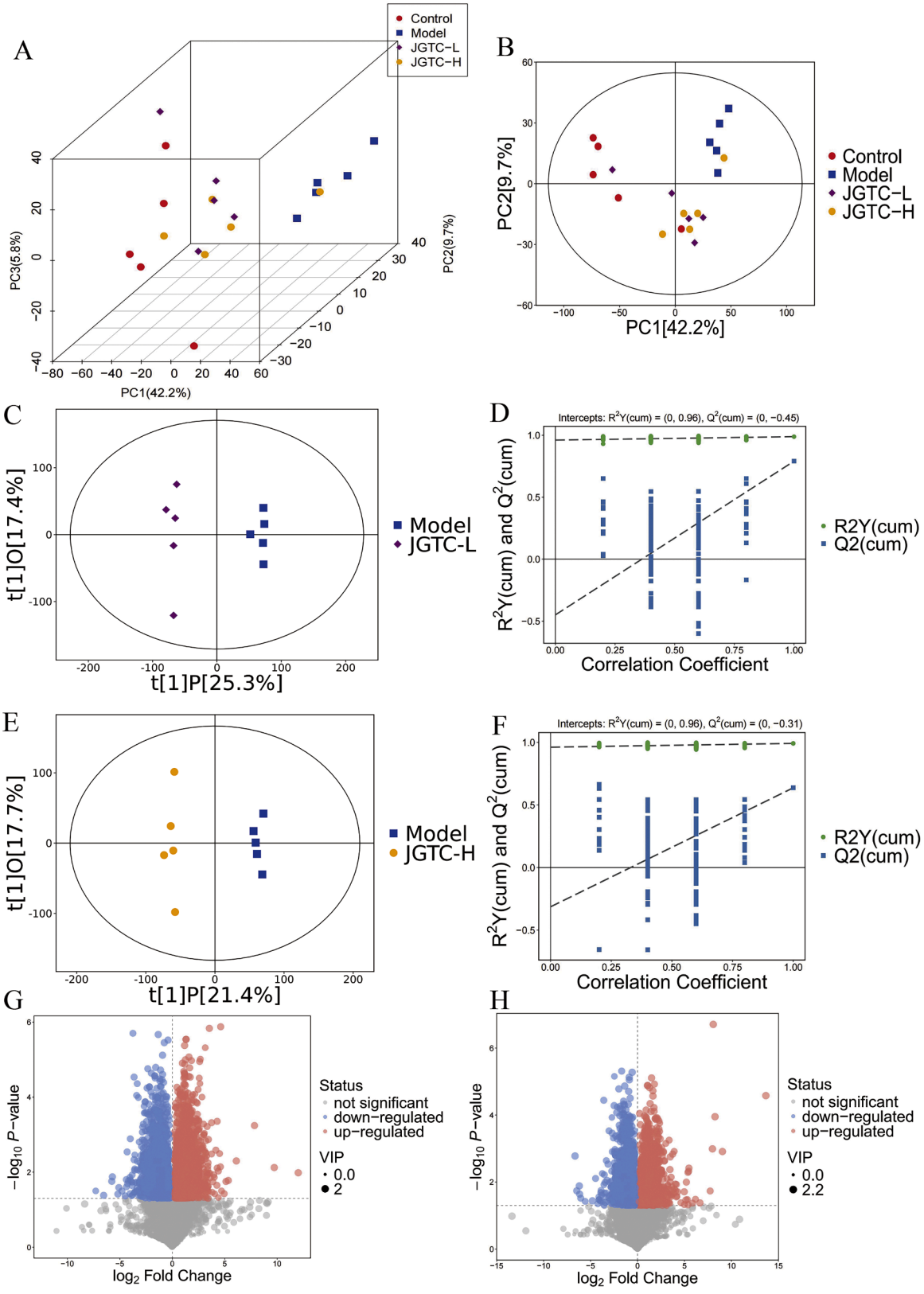

Fig. 4. Assessment of liver metabolites by untargeted metabolomics. Scatter plots of PCA scores. 3D plot (A) and 2D scatter plots (B). OPLS-DA score plot (B and E). Corresponding validation plot from OPLS-DA (D and F). Volcano plot of differential fecal metabolites between the model and JGTC-L (G) and JGTC-H groups (H).

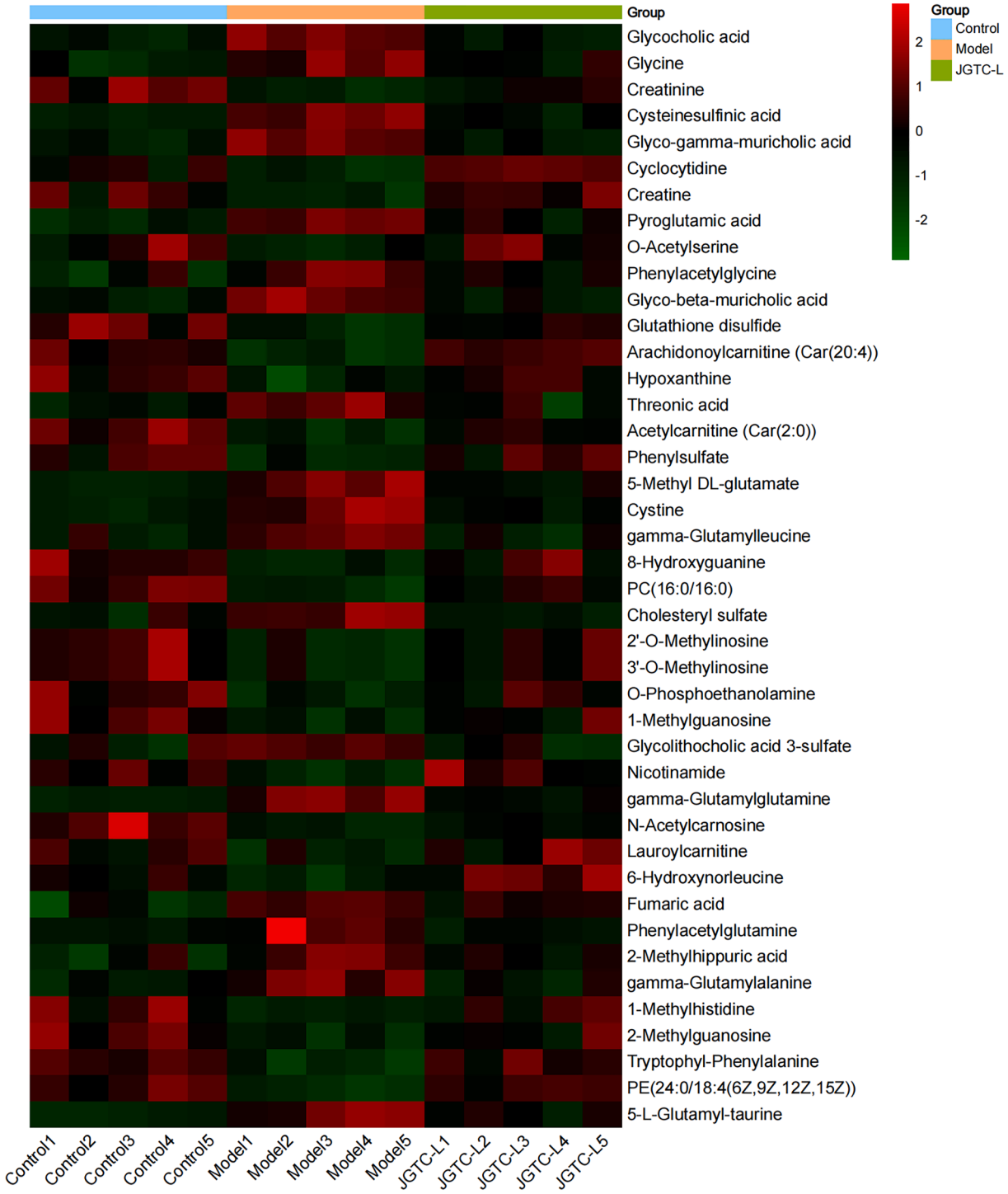

Fig. 5. Heatmap of significantly different liver metabolites between the control, model, and JGTC-L groups. The relative expression of liver metabolites is represented by different colors ($n = 5$ per group).

(MeOH:ACN:H2O, 2:2:1 [v/v], 500 mL) was mixed with liver tissue samples of the mice (25 mg). Protein precipitation was performed by vortexing the mixed solution for 30 s, sonicating it for 10 min at 4 °C, and incubating it for 1 h at −40 °C. Supernatant from the centrifuged samples was transferred to a fresh glass vial for analysis after centrifugation for 15 min at 13,800 × *g* at 4 °C.

Serum and fecal sample preparation, ultrahigh-performance liquid chromatography Quadrupole-Orbitrap tandem mass spectrometry (UHPLC-Q-Orbitrap MS) analyses, data preprocessing, and the annotation of serum, liver, and fecal metabolomics were performed as previously described (Zhang et al., 2022a).

Statistical analysis

All statistical analyses were performed using SPSS 22.0 and GraphPad Prism version 8.0 software. The data are expressed as the mean ± standard error of the mean (SEM). Differences between groups of data were evaluated by one-way analysis of variance (ANOVA). $P < 0.05$ was set as the threshold for statistical significance.

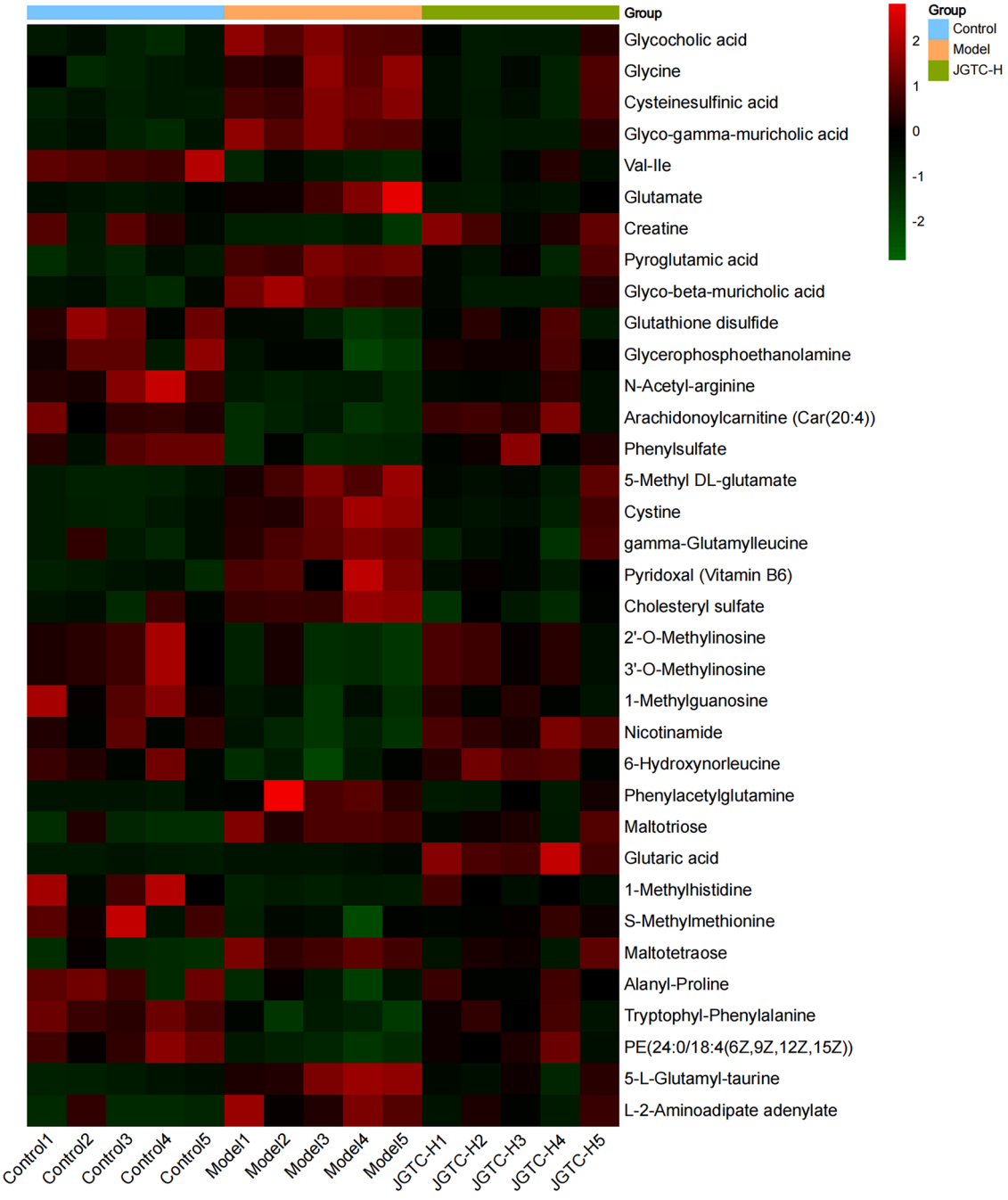

Fig. 6. Heatmap of significantly different liver metabolites between the control, model, and JGTC-H groups. The relative expression of liver metabolites is represented by different colors ($n = 5$ per group).

Results

Chemical components of JGTC

We used UPLC-Q-TOF/MS/MS to systematically investigate the collision patterns of the primary constituents of JGTC, resulting in the identification of 33 compounds in the negative mode, which are presented in Table 1 and, among the 33 compounds, there were 21 compounds detected in the positive mode, which are presented in Supplementary Table 2 and Supplementary Fig. 1.

Effect of JGTCs on streptozotocin-induced diabetic rats

We established a diabetic rat model by the intraperitoneal injection of STZ and administration of an HFD to investigate the effects of JGTCs on diabetes. Compared to the control group, the levels of FBG, PBG, and glucose AUC were increased significantly in the diabetic rats (model group) ($P < 0.05$ and $P < 0.01$; Fig. 1A–C). JGTC treatment significantly decreased FBG, PBG, and glucose AUCs ($P < 0.05$ and $P < 0.01$, Fig. 2) compared to the model group.

The liver histology of rats in the control group was normal. In contrast, rats in the model group showed lipid accumulation, which is typically observed in diabetes (Fig. 2D). Compared to the model group, liver histological changes were significantly improved in the JGTC-L and JGTC-H groups. H&E staining showed that JGTC treatment decreased cytoplasmic fat vacuoles and ballooning degeneration compared to the model group. In addition, Oil Red O staining confirmed that JGTCs inhibited lipid droplet accumulation in liver tissues. The levels of TC,

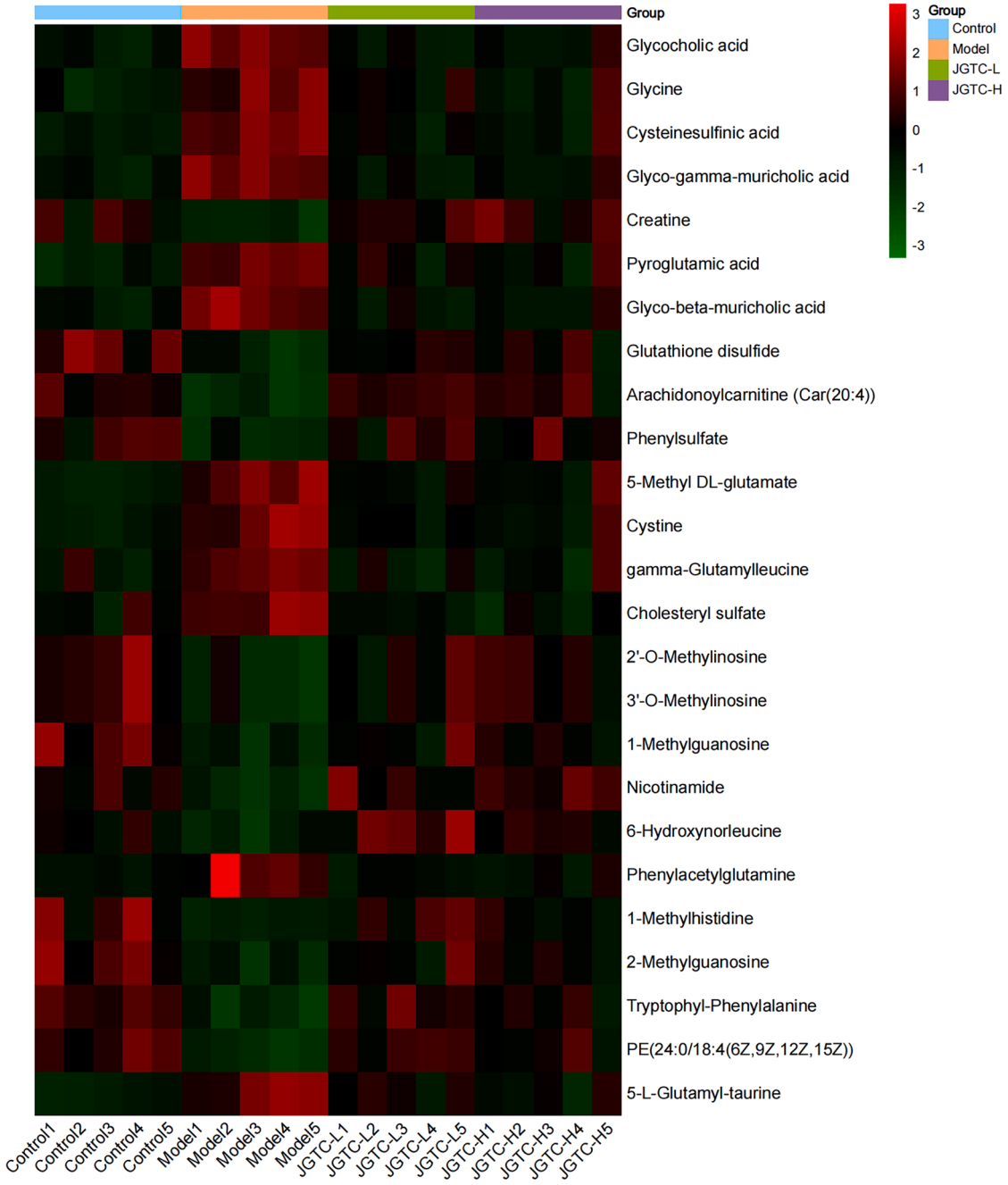

Fig. 7. Comparative abundance of significant differential liver metabolites in the control, model, JGTC-L, and JGTC-H groups.

TG, and LDL-C were significantly increased in the model group ($P < 0.05$ and $P < 0.01$, Fig. 2E–G), and these levels were significantly decreased by JGTC treatment ($P < 0.05$ and $P < 0.01$, Fig. 2E–G). The liver injury index test results revealed that the ALT and AST levels were significantly increased in the model group ($P < 0.05$ and $P < 0.01$, Fig. 2H, I), and these effects were also significantly improved by SC treatment ($P < 0.05$ and $P < 0.01$, Fig. 2H, I).

JGTC regulates hepatic FXR expression in diabetic rats and reduces lipid accumulation and the inflammatory response. FXR has been identified as an important regulator of diabetes, with the ability to alleviate the condition and its complications by regulating blood glucose levels, lipid metabolism, and inflammatory response (Qin et al., 2020). Our results showed that JGTCs also regulated blood glucose and lipid metabolism and alleviated liver injury in diabetic rats ($P < 0.05$ and $P < 0.01$, Fig. 2). Next, we evaluated the ability of JGTCs to protect against diabetes in rats by regulating FXR activity. As expected, we found that FXR expression was downregulated in the liver of diabetic rats, and this effect was alleviated by JGTC treatment ($P < 0.05$ and $P < 0.01$, Fig. 3A, B). We also analyzed several genes involved in lipid metabolism. *CYP7A1, Srebp-1c,* and *FAS* expression were upregulated in diabetic rats, and this effect was reversed by JGTC treatment ($P < 0.05$ and $P < 0.01$, Fig. 3C–E). Considering the anti-inflammatory effects of FXR, we examined the expression of immune factors in diabetic rats. Compared with the control group, the expression of tumor necrosis factor (TNF)-α, interleukin (IL)-6, and IL-1β was upregulated in model rats, and this effect was alleviated by JGTC treatment ($P < 0.05$ and $P < 0.01$, Fig. 3F–H).

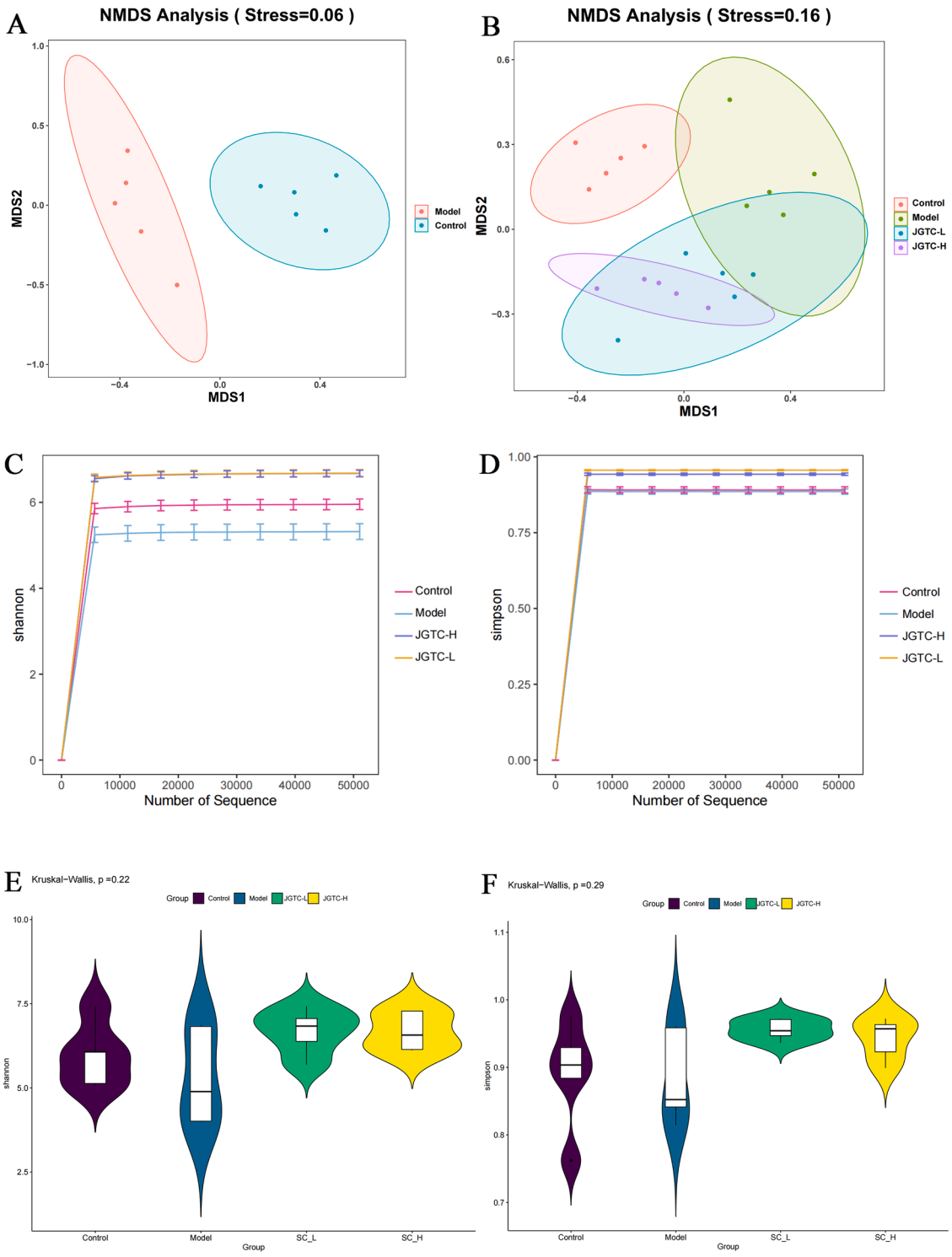

Fig. 8. α and β-Diversity analyses of intestinal microbiota in the control, diabetic, JGTC-L, and JGTC-H groups. NMDS analysis of control and model group (A) and NMDS analysis of the 4 groups (B). Rarefaction curves of the Shannon index (C) and the Simpson index (D). α-Diversity in the Shannon index (E), and the Simpson index (F).

JGTC alters liver metabolite composition in DM rats

The liver is an important regulatory organ for bile acid, glucose, and lipid metabolism. Bile acid is an endogenous ligand of FXR, and metabolic changes in bile acid can affect the expression and function of FXR. We analyzed the liver metabolic profiles of the control, model, JGTC-L, and JGTC-H groups using untargeted metabolomics techniques to explore the relationship between FXR and liver bile acid metabolism in diabetic rats after JGTC treatment. The principal component analysis (PCA) score plot showed a clear separation among the four groups, with the JGTC-L and JGTC-H samples located between the control and model groups (Fig. 4A and B).

After PCA, supervised orthogonal partial least squares-discriminant analysis (OPLS-DA) was applied to identify metabolites. The liver OPLS-DA score plots of pairs of groups (model vs. JGTC-L or model vs. JGTC-H) are shown in Fig. 4C and E. The established OPLS-DA models

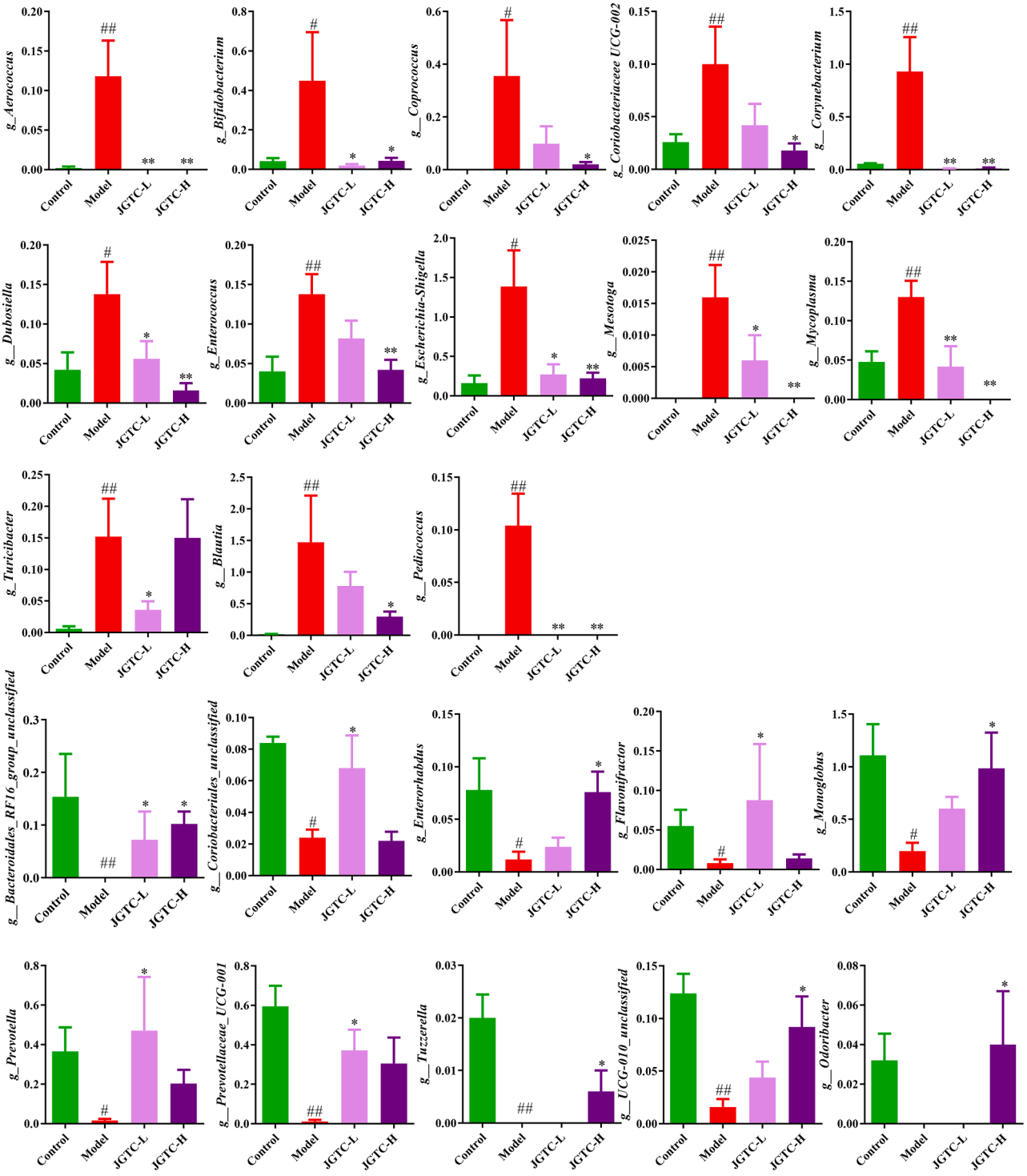

Fig. 9. Changes in species abundance at the genus level in the 4 groups. $^{\#}P < 0.05$, $^{\#\#}P < 0.01$, vs. the control group; $^{*}P < 0.05$, $^{**}P < 0.01$, vs. the model group.

were identified by 200 response permutation testing (Fig. 4D–F). In the comparison of the model and JGTC-L groups, $R^2Y = 0.96$, $Q^2 = -0.45$. In the comparison of the model and JGTC-H groups, $R^2Y = 0.96$, $Q^2 = -0.31$. The differential liver metabolites are illustrated in the volcano plots shown in Fig. 4G and H.

Metabolites were identified by variable importance in the projection (VIP) values (threshold >1) of OPLS-DA and *P*-values (threshold < 0.05) in the Student's *t*-test. We found 114 differential metabolites between the control and model groups (Supplementary Fig. 2), 52 between the model and JGTC-L groups (Supplementary Fig. 3), and 43 between the model and JGTC-H groups (Supplementary Fig. 4). 43 differential metabolites were found among the control, model, and JGTC-L groups (Fig. 5). Thirty-six metabolites were found among the control, model, and JGTC-H groups (Fig. 6), and 26 differential metabolites among the control, model, JGTC-L and JGTC-H groups, as presented in Fig. 7. We detected a significant number of bile acid metabolites associated with FXR, such as glyco-beta-muricholic acid, glycocholic acid, tauro-beta-muricholic acid, and tauro-gamma-muricholic acid. Compared with the control group, the levels of glyco-beta-muricholic acid and glycocholic acid were increased significantly in model rats, and the levels of

the two bile acid metabolites were decreased in the JGTC-L and JGTC-H group. The levels of tauro-beta-muricholic acid and tauro-gamma-muricholic acid were higher in the model group than in the JGTC-L group.

JGTC improves intestinal flora disorder in DM rats

We analyzed the 16S rDNA of rats in the control, diabetic, JGTC-L, and JGTC-H groups to determine how JGTC affects gut microbial communities and compared microbial species in different samples using non-metric multidimensional scaling (NMDS) based on beta diversity analysis. We detected a large variability in the control and model groups, with those in the JGTC group closer to those in the control group (Fig. 8A and B). Shannon and Simpson indices were used to reflect the diversity of the sample population. Compared with the control group, the Shannon and Simpson indices of the model group were decreased, whereas the two indices of the JGTC-L and JGTC-H groups were higher than those of the model group (Fig. 8C–F). Phylum, class, order, family, and genus information are provided in Supplementary Figs. 5–9. Differences between the 4 groups at the genus levels were evaluated by ANOVA and the results are shown in Fig. 9.

At the genus level, the relative abundance of *g_Aerococcus, g_Bifidobacterium, g_Coprococcus, g_Coriobacteriaceae_UCG-002, g_Corynebacterium, g_Enterorhabdus, g_Escherichia-Shigella, g_Mesotoga, g_Mycoplasma, g_Dubosiella, g_Pediococcus, g_Blautia*, and *g_Turicibacter* was significantly increased in the model group compared with the control group ($P < 0.05$ and $P < 0.01$, Fig. 9), whereas the relative abundance of *g_Coriobacteriales_unclassified, g_Enterorhabdus, g_Flavonifractor, g_Monoglobus, g_Prevotella, g_Prevotellaceae_UCG-001, g_Tuzzerella, g_UCG-010_unclassified, g_Bacteroidales_RF16_group_unclassified*, and *g_Odoribacter* was decreased ($P < 0.05$ and $P < 0.01$, Fig. 9). JGTC administration significantly reversed the differences observed at the genus level in the model group, resulting in intestinal microflora relative abundance levels similar to those in the control group ($P < 0.05$ and $P < 0.01$).

We analyzed all validated sequences using the linear discriminant analysis effect size (LEfSe) method to determine which phylotypes were significantly modulated in the model group and the effect of JGTC treatments. Discriminative features were identified based on an linear discriminant analysis (LDA) score of >3.0 (Supplementary Figs. 10 and 11). In accordance with the changes observed at the genus level, phyla such as *g_Blautia, g_Escherichia-Shigella, g_Corynebacterium, g_Marvinbryantia, g_Bifidobacterium, g_Coprococcus, g_Kroppenstedtia*, and *g_Pediococcus* were enriched in the model group compared with the control group.

JGTC alters fecal metabolite composition in DM rats

Small molecules are used as bridges for substance and information exchange between the gut microbiota and the host. Alterations in the intestinal flora are reflected by changes in the metabolism of substances. Therefore, we assessed the metabolic functionality of the gut microbiota by analyzing fecal samples to investigate potential changes in the intestinal microbiota.

UHPLC-Q-Orbitrap MS was used to analyze fecal samples from rats in the control, model, JGTC-L, and JGTC-H groups, and unsupervised PCA was performed to visualize the general clustering of the samples. PCA plots of all fecal samples showed clear group distinctions (Supplementary Fig. 12A and B). The JGTC-L and JGTC-H samples were closer to the control group than the model group. All fecal samples fell within the 95 % confidence interval. After PCA, supervised OPLS-DA was applied to identify the metabolites. The OPLS-DA score plots of pairs of groups (model vs. JGTC-L or model vs. JGTC-H) are shown in Supplementary Fig. 12C and E. Permutation tests of 200 responses were used to identify the established OPLS-DA models (Supplementary Fig. 12D and F). The model quality was estimated by R^2Y and Q^2 values. The differential fecal metabolites are illustrated in the volcano plots shown in Supplementary Fig. 12G and H.

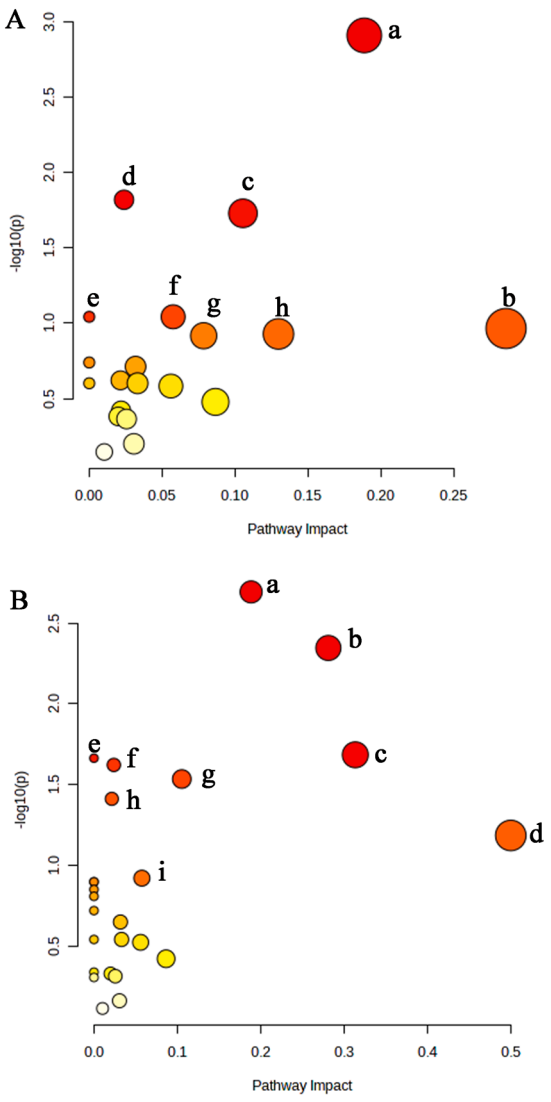

Fig. 10. Summary of the pathways altered by JGTC-L treatment (A). a: Histidine metabolism, b: taurine and hypotaurine metabolism, c: tryptophan metabolism, d: arginine and proline metabolism, e: arachidonic acid metabolism, f: glycerophospholipid metabolism, g: vitamin B6 metabolism, and h: tyrosine metabolism. Summary of the pathways altered by JGTC-H treatment (B). a: Histidine metabolism, b: tyrosine metabolism, c: arachidonic acid metabolism, d: phenylalanine, tyrosine, and tryptophan biosynthesis, e: arginine bio synthesis, f: arginine and proline metabolism, g: tyrosine metabolism, h: pantothenate and CoA biosynthesis, and i: glycerophospholipid metabolism.

Based on the above analysis, JGTC-L altered 142 key metabolites in model rats (Supplementary Fig. 13). These metabolites were enriched in the metabolism of histidine, taurine and hypotaurine, tryptophan, arginine and proline, arachidonic acid, glycerophospholipids, vitamin B6, and tyrosine (Fig. 10A). JGTC-H altered 165 key metabolites in the model rats (Supplementary Fig. 14), and these metabolites were enriched in histidine metabolism, tyrosine metabolism, arachidonic acid metabolism, phenylalanine, tyrosine and tryptophan biosynthesis, arginine biosynthesis, and arginine and proline metabolism (Fig. 10B). A Venn diagram of the differential metabolites in the JGTC-L and JGTC-H groups (Supplementary Fig. 15) revealed 114 shared fecal metabolites (Fig. 11).

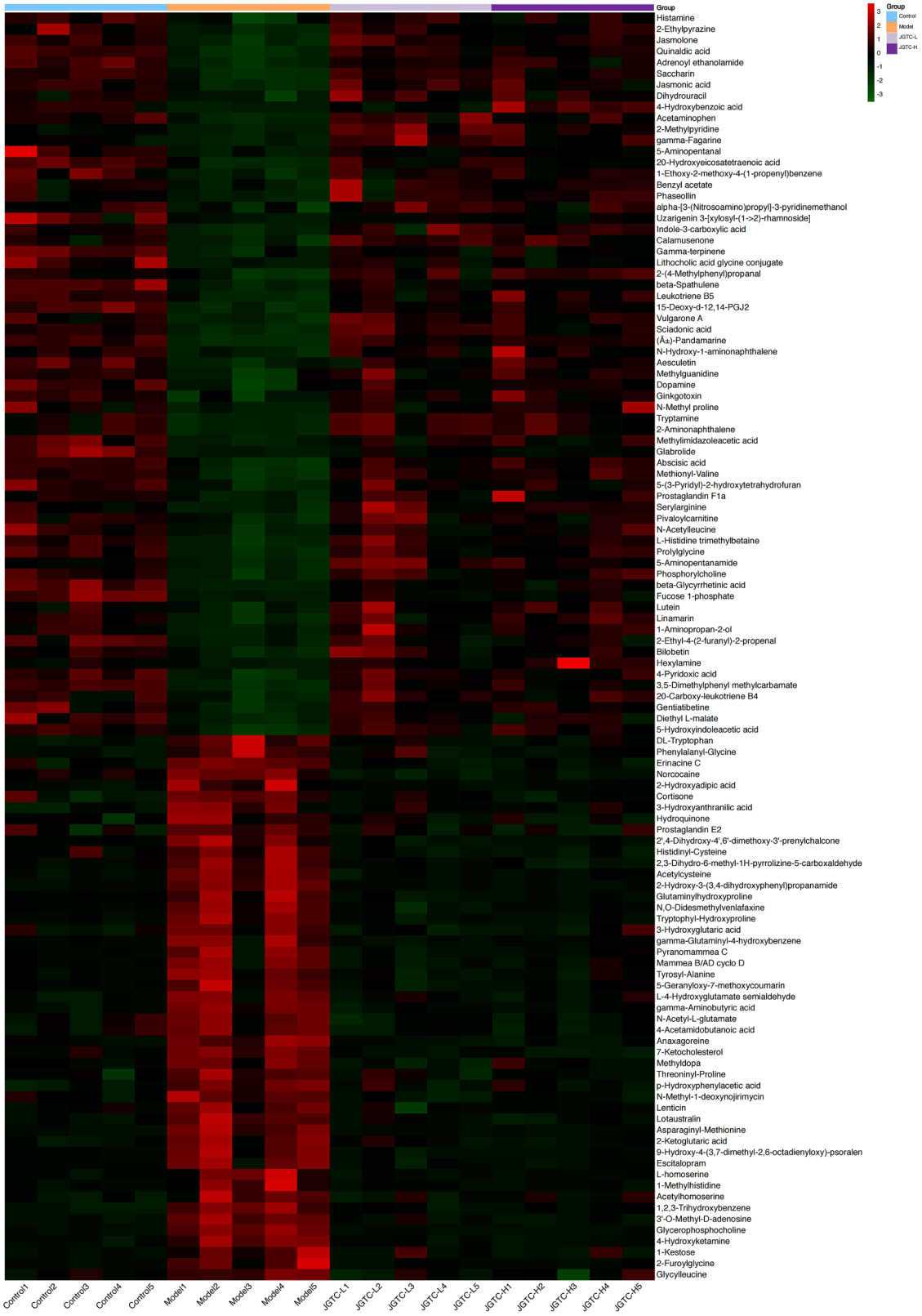

Fig. 11. Comparative abundance of significant differential fecal metabolites in the control, model, JGTC-L, and JGTC-H groups.

JGTC alters serum metabolite composition in DM rats

Changes in the composition of the blood reflect metabolism and health. Therefore, we also analyzed the serum metabolic profiles of rats in the control, model, JGTC-L, and JGTC-H groups using untargeted metabolomics techniques. The PCA score plot showed a clear separation among the 4 groups (Supplementary Fig. 16A and B), with the JGTC-L and JGTC-H samples located between the control and model groups.

Metabolites were identified using supervised OPLS-DA after PCA. The serum OPLS-DA score plots of pairs of groups (model vs. JGTC-L or

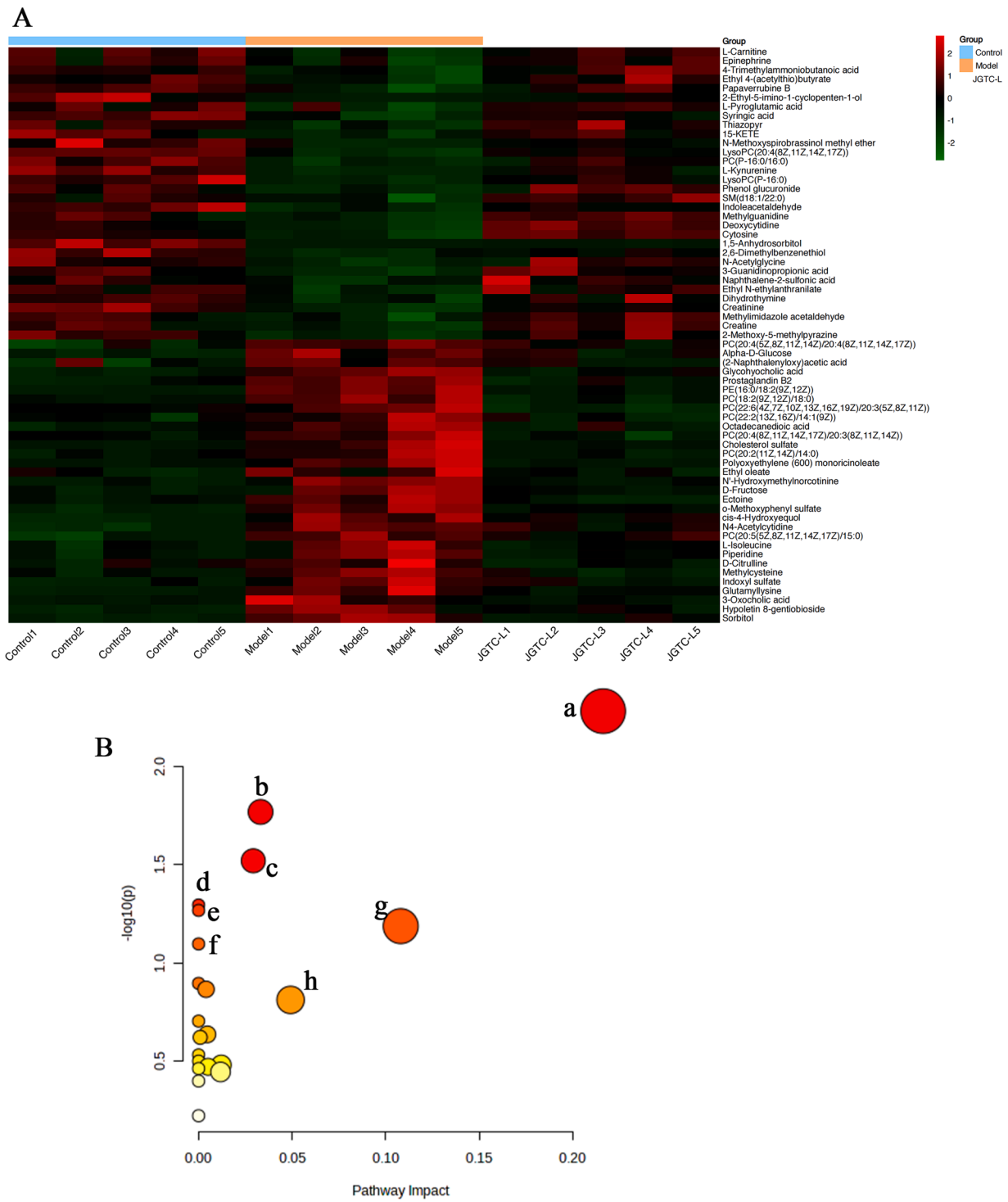

Fig. 12. Serum metabolites and pathways significantly modulated by JGTC-L. Comparison of the relative abundance of serum metabolites in the control, model, and JGTC-L groups (A). Summary of the pathway analysis (B). a: Glycerophospholipid metabolism, b: fructose and mannose metabolism, c: galactose metabolism, d: linoleic acid metabolism, e: amino sugar and nucleotide sugar metabolism, f: valine, leucine, and isoleucine biosynthesis, g: tryptophan metabolism, and h: histidine metabolism.

model vs. JGTC-H) are shown in Supplementary Fig. 16C and E. The established OPLS-DA models were identified by 200 response permutation testing (Supplementary Fig. 16D–F). In the comparison of the model and JGTC-L groups, $R^2Y = 0.95$, $Q^2 = -0.45$. In the comparison of the model and JGTC-H groups, $R^2Y = 0.96$, $Q^2 = -0.41$. The differential serum metabolites are illustrated in the volcano plots shown in Supplementary Fig. 16G and H.

JGTC-L altered 63 key metabolites in model rats (Fig. 12A, Supplementary Table 3) and these metabolites were enriched in the metabolism of glycerophospholipids, fructose and mannose, galactose, linoleic acid metabolism, amino sugars and nucleotide sugars, tryptophan, and histidine, as well as valine, leucine, and isoleucine biosynthesis (Fig. 12B). JGTC-H altered 49 key metabolites in model rats (Fig. 13A, Supplementary Table 4) and these metabolites were enriched

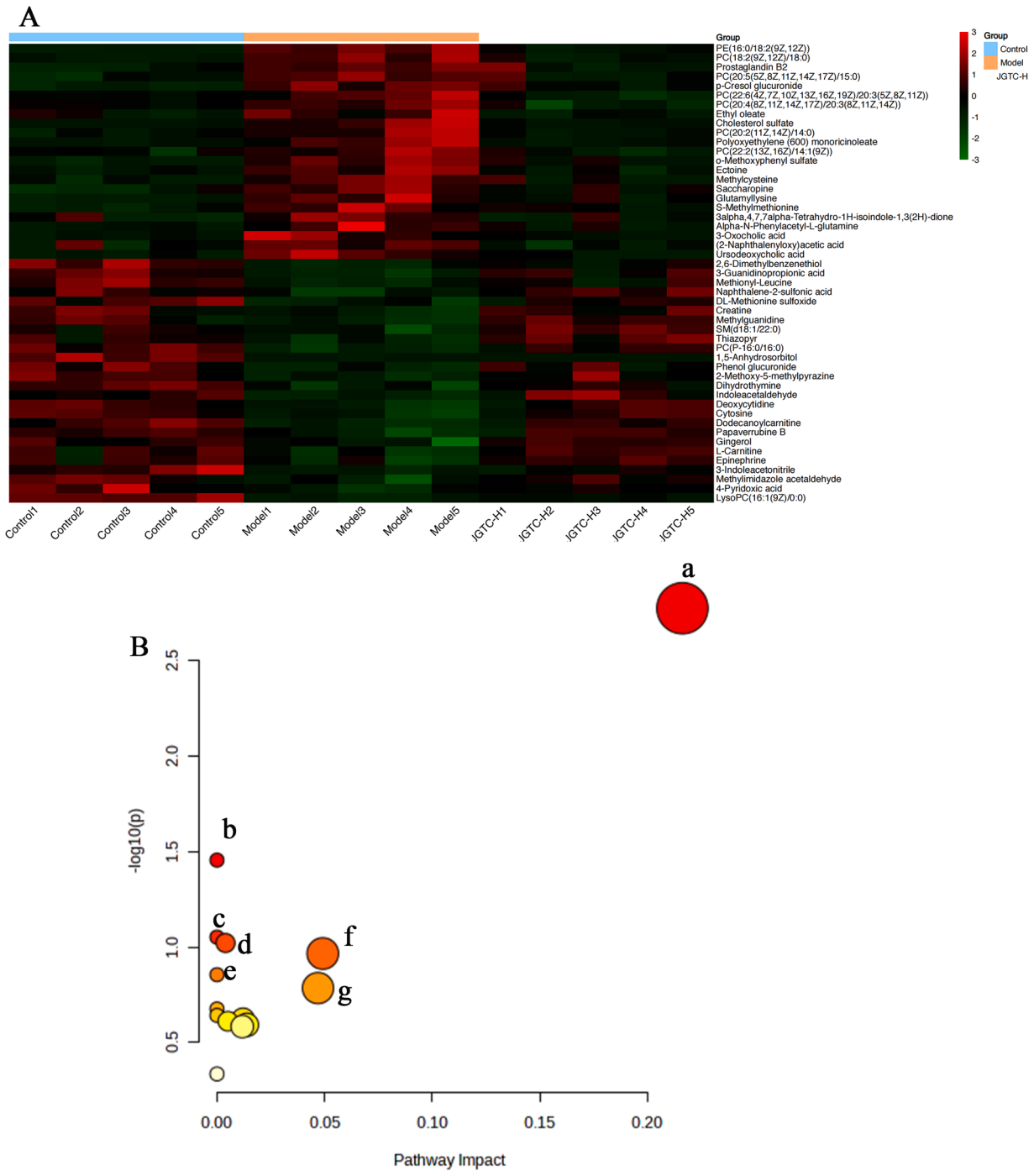

Fig. 13. Serum metabolites and pathways significantly modulated by JGTC-H. Comparison of the relative abundance of serum metabolites in the control, model, and JGTC-H groups (A). Summary of the pathway analysis (B). a: Glycerophospholipid metabolism, b: linoleic acid metabolism, c: alpha-linolenic acid metabolism, d: glycosylphosphatidylinositol-anchor biosynthesis, e: sphingolipid metabolism, f: histidine metabolism, and g: lysine degradation.

in the metabolism of glycerophospholipids, linoleic acid, alpha-linolenic acid, sphingolipids, and histidine, as well as glycosylphosphatidylinositol-anchor biosynthesis and lysine degradation. A Venn diagram of the differential metabolites in the JGTC-L and JGTC-H groups (Supplementary Fig. 17) revealed 36 shared serum metabolites (Fig. 14).

Correlation between intestinal flora and metabolites

Spearman's correlation analysis was used to examine the relationship between altered fecal metabolites and the gut microbiota (top 30). Heatmaps of the results are shown in Fig. 15. Specifically, *g_Tuzzerella* was associated with 26 fecal metabolites; *g_Prevotellaceae_UCG-001* and *g_Flavonifractor* were associated with 24 fecal metabolites; *g_Aerococcus* and *g_UCG-010_unclassified* were associated with 25 fecal metabolites; *g_Monoglobus* and *g_Coprococcus* were associated with 23 fecal metabolites; *g_Corynebacterium*, and *g_Mycoplasma* were associated with 21 and 22 fecal metabolites, respectively; *g_Coriobacteriaceae_UCG-002, g_Blautia*, and *g_Odoribacter* were each associated with 18 fecal metabolites; *g_Enterococcus, g_Mesotoga*, and *g_Pediococcus* were each associated with 16 fecal metabolites; *g_Bifidobacterium, g_Prevotella*, and *g_Bacteroidales_RF16_group_unclassified* were each associated with 17 fecal metabolites;

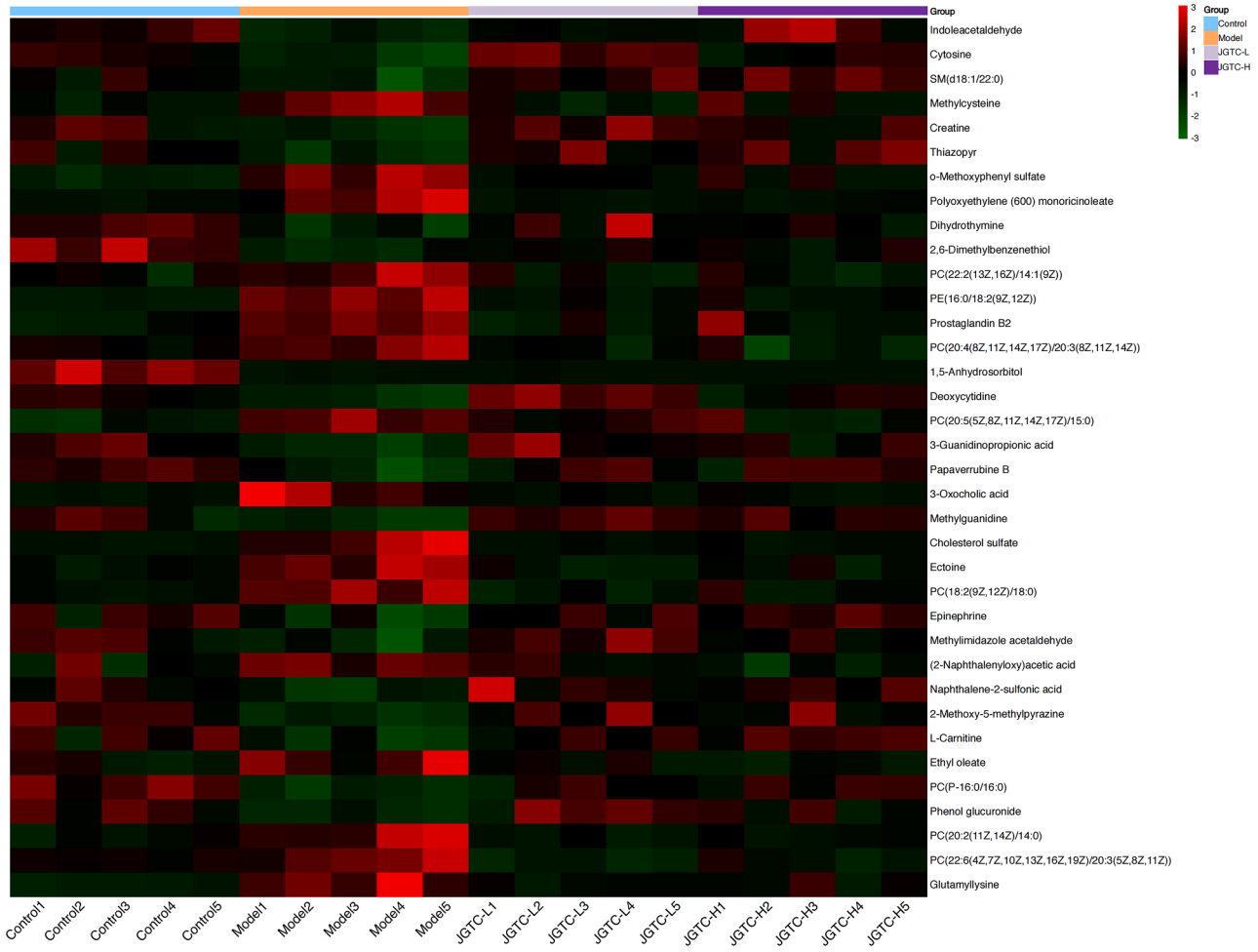

Fig. 14. Comparative abundance of significant differential serum metabolites in the control, model, JGTC-L, and JGTC-H groups.

g_Turicibacter, *g_Escherichia-Shigella*, and *g_Coriobacteriaceae_UCG-002* were associated with 13, 14, and 9 fecal metabolites, respectively; and *g_Dubosiella* and *g_Enterococcus* were each associated with 10 fecal metabolites. With the exception of oleamide, all fecal metabolites were significantly correlated with at least one genus. Spearman's correlation analysis showed a strong correlation between the differential metabolic profiles of feces and serum (Supplementary Fig. 18).

Discussion

In our study, a diabetic rat model was established using an HFD and STZ to investigate the role of JGTCs. Treatment with JGTCs alleviated the symptoms associated with hyperglycemia and hyperlipidemia and protected model rats from lipid metabolism disorders. The mechanism underlying the effects of JGTCs in this model may be due to its ability to regulate the structure of the intestinal microbiota (by altering the relative abundances of 22 genera, including *g_Aerococcus, g_Bifidobacterium, g_Coprococcus, g_Coriobacteriaceae_UCG-002*, and *g_Corynebacterium*) and thus, affect FXR and inflammatory factors, and prevent changes in some key fecal, serum, and liver metabolites. These findings implicate JGTCs as a potential therapeutic agent for hyperglycemia and hyperlipidemia.

DM is also commonly associated with disturbances in lipid metabolism, which typically determine the course and severity of the disease (Yang et al., 2019). Our study showed that diabetic rats had significantly higher blood glucose levels, along with higher TC, TG, and LDL-C levels, which confirmed the existence of disrupted lipid metabolism in the DM model rats. Following a 4-week administration of JGTCs, serum blood glucose and lipid levels were significantly decreased. Previous studies in HFD-fed mice showed that the ethanol extract of *Smilax china* reduced cholesterol biosynthesis, reduced plasma and liver cholesterol concentrations, and enhanced TG lipase activity (Yudhani et al., 2023). In our current study, we found that the JGTC extract solution had similar effects in DM rats induced by STZ administration and an HFD (Yudhani et al., 2023). Hepatocyte function can be impaired by DM and its complications (Yan et al., 2022). The histopathological observations were consistent with the biochemical observations in serum. These results indicate that JGTCs exert hypoglycemic effects and regulate lipid metabolism to decrease the liver injury associated with DM in model rats.

The liver regulates blood glucose and lipid metabolism by responding to insulin signals and is an important site of glucose and lipid metabolism. FXR, an important regulator of metabolism, is highly expressed in the liver. CYP7A1 is a downstream target gene of FXR, which is involved in bile acid and lipid metabolism. Jiang et al. found that baicalin inhibited CYP7A1 expression in the liver of diabetic mice to reduce lipid accumulation (Jiang et al., 2007). In our study, FXR expression in the liver of diabetic rats was downregulated, and this effect was reversed by JGTC treatment. JGTC also inhibited the up-regulation of CYP7A1 and lipid accumulation-related genes Srebp1 and FAS in the liver of diabetic rats. FXR has been reported to alleviate diabetes-induced nonalcoholic fatty liver disease by regulating the inflammatory response (Hu et al., 2018). Our study found that pro-inflammatory factors (IL-β, TNF-α, IL-6) were improved in diabetic rats. Our results also showed that JGTC treatment inhibited pro-inflammatory factors (IL-β, TNF-α, and IL-6) in the liver of diabetic rats and alleviated liver injury. These results suggest that FXR may be a

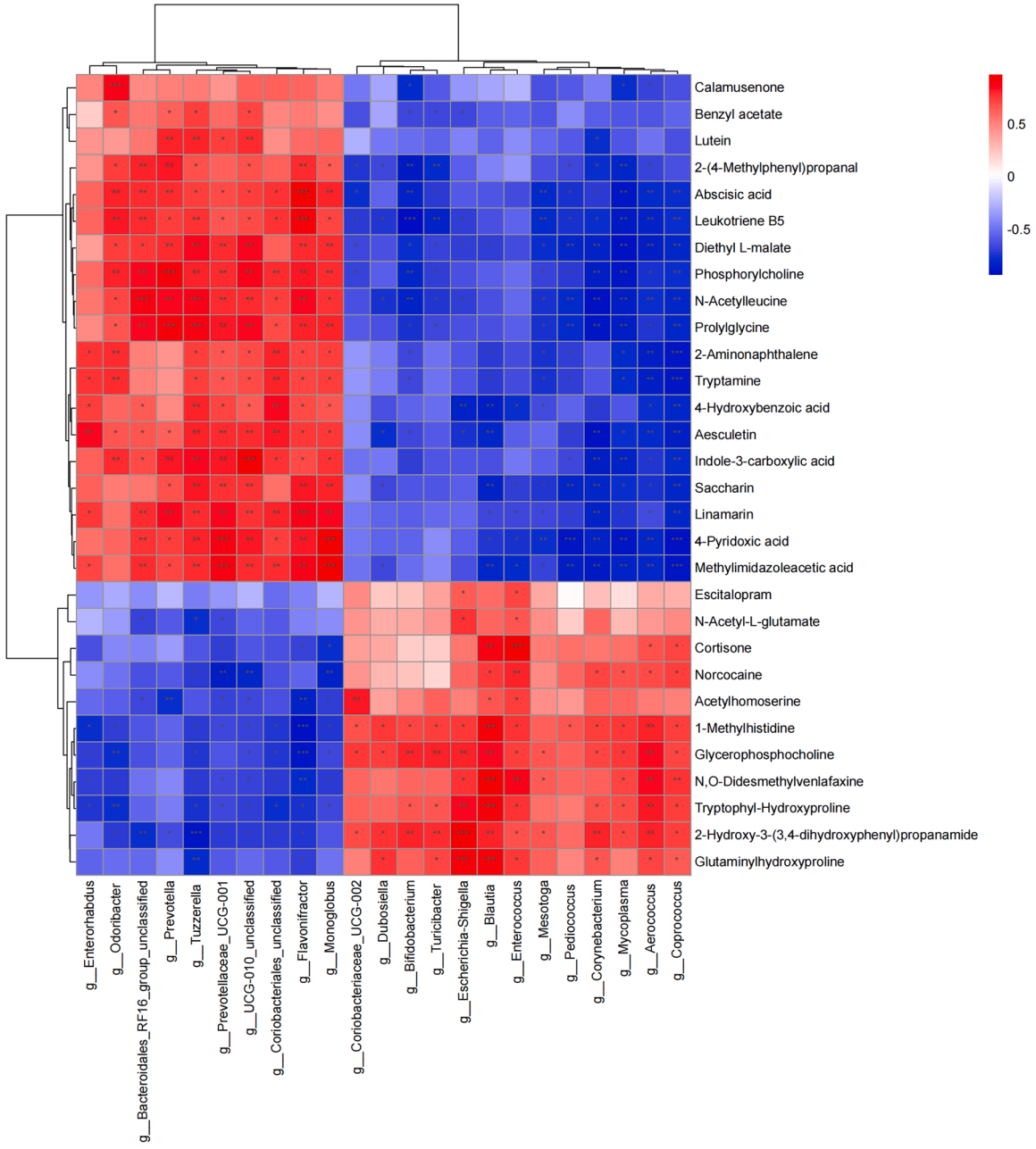

Fig. 15. Correlation analysis of the top 30 significant changes in fecal metabolites by bacterial strain (by genus). Positive and negative correlations in the heatmap are shown in red and blue, respectively (*$P < 0.05$, **$P < 0.01$, ***$P < 0.001$).

potential target for JGTCs in alleviating liver injury in diabetic rats.

Disordered gut microbiota composition manifests as intestinal inflammation and impaired intestinal tight junction with higher permeability, leading to peripheral inflammation, and, ultimately, the development of diabetes. Previous studies reported that FXR not only inhibited the activity of nuclear factor (NF)-κB to protect hepatocytes from inflammatory damage but also regulated glycolipid metabolism and alleviated diabetes-induced nonalcoholic fatty liver (Hu et al., 2018; Shiragannavar et al., 2023; Valencia-Ortega et al., 2023). Our results also showed that JGTC treatment promoted the expression of FXR in the liver of diabetic rats and inhibited the expression of adipokines (Srebp1c and Fas) and pro-inflammatory factors (IL-β, TNF-α, and IL-6) to alleviate liver injury. These results indicate that JGTCs may regulate liver inflammation and glucose and lipid metabolism in diabetic rats through FXR. However, further exploration is needed.

Considering that bile acid is an endogenous ligand of FXR, its metabolic changes will affect the expression and function of FXR. Therefore, we performed a metabolomics analysis of the liver and found that some bile acid metabolites were abnormal. Glyco-beta-muricholic acid is a bile acid and a potent, selective, and oral bioactive inhibitor of the FXR (Jiang et al., 2015). In our study, the content of glyco-beta-muricholic acid was higher in the model group, and the levels of tauro-gamma-muricholic acid were decreased in the JGTC-L and JGTC-H groups.

To explore the diversity of the gut microbiota in rats, we analyzed 16S rRNA sequences. Our results showed that the Shannon and Simpson indexes were decreased in DM rats compared with healthy rats and both indexes were improved following JGTC treatment. The control and model samples were clearly separated based on NMDS analysis, with the JGTC-L and JGTC-H samples located between them. Subsequently, LEfSe and one-way ANOVA analysis of the different intestinal microflora revealed that the levels of 13 genera were increased in the model group

compared with the control group, whereas 14 genera were decreased. JGTC treatment reversed the abundance of these flora to levels that were more similar to those in the control group. JGTC-H treatment altered 18 genera, and JGTC-L altered 14, with 8 genera, including *g_Aerococcus, g_Bifidobacterium*, and *g_Corynebacterium*, shared by the 2 groups.

The correct identification and treatment of *g_Aerococcus* is critical to avoid a life-threatening systemic infection (Cattoir et al., 2010). The abundance of *g_Blautia* is positively associated with DM (Gurung et al., 2020; Wang et al., 2021). Huang et al. also showed a higher abundance of *g_Blautia* in individuals with DM compared to healthy individuals (Huang et al., 2022). Our study found that DM rats had higher levels of *g_Blautia* than control rats, and JGTC treatment decreased this relative abundance of *g_Blautia*. Huang et al. reported an increased abundance of *g_Coprococcus* in a DM rat model (Huang et al., 2022). In this study, we found that JGTC treatment could reduce the abundance of *g_Coprococcus* in diabetic rats. The human microbiome is highly populated with *g_Prevotella* spp., which is a key player in the balance between health and disease (Tett et al., 2021). Some studies showed that the relative abundance of *g_Prevotella* and *g_Prevotellaceae_UCG-001* was lower in DM patients and animal models than in healthy controls (Zhang et al., 2023; Li et al., 2022). In accordance with previous studies, we also detected a decrease in the abundance of *g_Prevotella* and *g_Prevotellaceae_UCG-001* in the model group (Zhang et al., 2023; Li et al., 2022) and demonstrated that this was reversed after JGTC treatment. Changes in the abundance of *g_Dubosiella* in diabetes are controversial, with decreased abundance in the DM group in some studies (He et al., 2022; Yin et al., 2022; Zhou et al., 2023) and increased abundance in other studies (Zhang et al., 2022b; Wang et al., 2023). In our study, the abundance of *g_Dubosiella* was increased in the DM group (Zhang et al., 2022b; Wang et al., 2023). The presence of *g_Turicibacter* was increased in patients with severe fibrotic non-alcoholic fatty liver disease (NAFLD) (Rodriguez-Diaz et al., 2022). Another study showed that the abundance of Turicibacter was also increased in HFD-induced NAFLD (Somm et al., 2021). Other researchers also found that the abundance of *g_Turicibacter* was increased in diabetic mice (He et al., 2022; Shang et al., 2023). Our results are consistent with these previous studies. Our study demonstrated that the intestinal flora was changed in diabetic rats, and JGTC treatment regulated the balance of the intestinal flora to increase beneficial bacteria and reduce harmful bacteria.

The microbiota in the intestine is crucial to regulating the physiological functions of the host, particularly metabolic homeostasis. Untargeted metabolomics analysis can be used to highlight the gut microbiota metabolites that can be used to infer the co-metabolism of the host and the microbiome (Griffiths et al., 2010). We found that histidine metabolism, glycerophospholipid metabolism, and tryptophan metabolism, which are closely related to the abundance of the intestinal flora, were altered by JGTC treatment. Histamine, 1-methylhistidine, and methylimidazole acetic acid are crucial components of histidine metabolism. In each target organ, histamine signals H1Rs and H2Rs to regulate metabolic and inflammatory processes (Thangam et al., 2018). In our study, fecal histamine levels were decreased in the DM model group, whereas the levels of 1-methylhistidine and methylimidazole acetic acid were increased. After the administration of JGTCs, these metabolites returned to levels that were similar to those detected in the control group. In accordance with our fecal metabolomics data, our serum metabolomics analysis also showed that JGTCs regulate histidine metabolism. In our study, fecal histamine levels were decreased in the DM model group, whereas the levels of 1-methylhistidine and methylimidazole acetic acid were increased. The levels of these metabolites returned to control levels after JGTC administration. In accordance with our fecal metabolomics data, our serum metabolomics analysis also showed that JGTCs regulated histidine metabolism. Previous studies identified *g_Aerococcus, g_Bifidobacterium*, and *g_Dubosiella* as common flora associated with histidine metabolism (Wang et al., 2022; Liao et al., 2023). In addition, Liao et al. found that *g_Dubosiella* abundance was increased in NAFLD and affected histidine metabolism (Liao et al., 2023). We also found an increased abundance of *g_Dubosiella* and altered histidine metabolism in diabetic rats with fatty liver, the result was consistent with the above study (Liao et al., 2023).

The metabolism of tryptophan can be affected by gut microbes and host interactions (Agus et al., 2018). In addition to neuronal function and metabolism, tryptophan metabolism affects inflammation, oxidative stress, immune responses, and intestinal homeostasis (Xue et al., 2023). Our results showed that tryptamine was positively associated with *g_Prevotellaceae_UCG-001, g_Monoglobus, g_Enterorhabdus*, and *g_Tuzzerella*, and negatively associated with 7 genera, including *g_Blautia, g_Aerococcus*, and *g_Coprococcus. G_Aerococcus* was negatively associated with tryptamine. Tryptamine, which stimulates serotonin secretion by enterochromaffin cells, also regulates intestinal motility and function (Yano et al., 2015). Study demonstrated that tryptamine has antibacterial and anti-inflammatory properties (Malik et al., 2019). In our study, the abundance of tryptamine was decreased in DM model rats, whereas the expression of inflammatory factors (IL-1β, TNF-α, and IL-6) and the level of *g_Aerococcus* were significantly increased in STZ-induced diabetic rats, consistent with a previous report (He et al., 2022). These effects were improved by JGTC treatment. Prevotella was found to accumulate phenylethylamine, tyramine, and tryptamine, while cadaverine and histamine accumulated in the latter (Fernandez-Cantos et al., 2024). Our results showed that *g_Prevotella* and *g_Prevotellaceae_UCG-001* were all positively associated with tryptamine.

Alpha-linolenic acid metabolism, glycerophospholipid metabolism, and linoleic acid metabolism are lipid metabolism pathways (Han et al., 2015). Disturbances in these lipid metabolic pathways in DM model rats are consistent with pharmacodynamic phenotyping studies that showed that hepatic lipid metabolism was disturbed in diabetic rats. In addition, these phospholipids are abundant in atherosclerosis and found in all major lipoproteins. Both plasma PC and sphingomyelin have been identified as independent risk factors for coronary heart disease (Jiang et al., 2000; Schlitt et al., 2006; Wang et al., 2011). We found that the serum levels of PC (22:6(4Z,7Z,10Z,13Z,16Z,19Z)/20:3(5Z,8Z,11Z)), PE (16:0/18:2(9Z,12Z)), and fecal glycerophosphocholine were increased in the DM group, whereas the level of fecal PC was decreased in the DM group, and JGTCs regulated the levels of all 4 of these metabolites. In DM model rats, arginine and proline metabolism was greatly enriched (Yang et al., 2023). In our study, we found that the levels of L-4-hydroxyglutamate semialdehyde and gamma-aminobutyric acid, which are the key metabolites in arginine and proline metabolism, were increased in DM model rats, and the levels of both metabolites were decreased in the JGTC-L and JGTC-H groups.

A few recent studies reported the potent antidiabetic properties of *Smilax china* L. in mice with alloxan-induced uracil disease by inhibiting a-glucosidase and increasing the liver glycogen content (Gan et al., 2016; Ma et al., 1998). However, studies on the anti-diabetic effects of JGTCs have not yet been reported in the literature. The prevalence of diabetic lipid metabolism disorders has increased annually. Therefore, it is important to find drugs with the ability to treat diabetic liver lipid metabolism disorders. As far as we know, our study is the first to report the anti-diabetic effects and mechanisms of JGTCs in a diabetic rat model. We showed that JGTCs can affect the FXR signaling pathway and alleviate hyperglycemia, liver lipid accumulation, and inflammatory responses, as well as intestinal flora and bile acid metabolism disorders in diabetic rats. The results of this study may provide a basis for the clinical application and secondary development of JGTCs.

However, the mechanism by which JGTCs modulate FXR signaling and whether factors, such as intestinal flora and bile acid metabolism, are regulated through FXR remain to be fully elucidated. In future studies, we will investigate the mechanism underlying the close association of FXR with gut flora and bile acids. We will also further explore the ability of JGTCs to alter the gut microbiota and bile acid metabolism in diabetic rats.

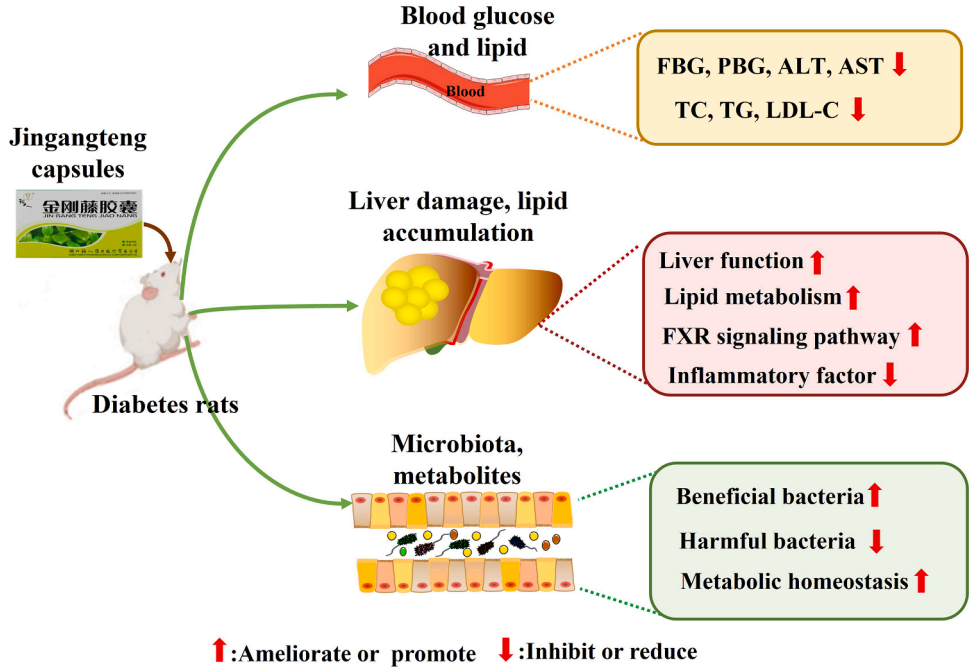

Fig. 16. Jingangteng capsules maintain metabolism and intestinal flora homeostasis in diabetic rats, and alleviates liver damage and lipid metabolism disorders in diabetic rats.

Conclusions

JGTCs were investigated in diabetic rats to determine their ameliorative effects on liver lipid disorders. As shown in Fig. 16, our results indicated that JGTC maintains metabolism and intestinal flora homeostasis in diabetic rats, and alleviates liver damage and lipid metabolism disorders in diabetic rats. Our findings revealed that the metabolism of histidine, glycerophospholipids, taurine and hypotaurine, tryptophan, arginine and proline, arachidonic acid, and linoleic acid was the key metabolic pathway involved in the effects of JGTCs. Our study highlights the potential of JGTCs for treating DM patients and uses in the design and secondary development of JGTCs.

Funding

This work was funded by the Hubei Natural Science and Technology Fund (No. 2023AFB513), the Open Fund of Hubei Key Laboratory of Resources and Chemistry of Chinese Medicine (No. KLRCCM2305), and Science Research Start-up Fund for Doctors of Hubei University of Science and Technology (BK202324, BK202336), China.

CRediT authorship contribution statement

Mi Chen: Writing – review & editing, Writing – original draft, Methodology, Conceptualization. **Manjun Gao:** Writing – original draft, Methodology, Data curation. **Hao Wang:** Validation, Software, Formal analysis. **Qingjie Chen:** Project administration, Methodology. **Xiufen Liu:** Methodology, Investigation. **Qigui Mo:** Project administration, Methodology. **Xingqiong Huang:** Software, Methodology. **Xiaochuan Ye:** Writing – review & editing, Resources, Conceptualization. **Dandan Zhang:** Writing – review & editing, Writing – original draft, Methodology, Funding acquisition, Conceptualization.

Declaration of competing interest

The authors declare that they have no conflict of interest.

Acknowledgments

We would like to thank MogoEdit (https://www.mogoedit.com) for English editing during the preparation of this manuscript. We thank Shanghai BIOTREE Biomedical Technology Co., Ltd for the technical support of gut microbiome sequencing and untargeted metabolomics analysis. We would like to thank the free online Oebiotech Cloud Platform (https://cloud.oebiotech.cn/task/).

Supplementary materials

Supplementary material associated with this article can be found, in the online version, at doi:10.1016/j.phymed.2024.155806.

References

Agus, A., Planchais, J., Sokol, H., 2018. Gut microbiota regulation of tryptophan metabolism in health and disease. Cell Host. Microbe 23, 716–724.
Baothman, O.A., Zamzami, M.A., Taher, I., Abubaker, J., Abu-Farha, MA.O., 2016. The role of gut microbiota in the development of obesity and diabetes. Lipids Health Dis. 15, 108–116.
Cattoir, V., Kobal, A., Legrand, P., 2010. Aerococcus urinae and Aerococcus sanguinicola, two frequently misidentified uropathogens. Scand. J. Infect. Dis. 42, 775–780.
Chen, M., Lu, C.L., Lu, H.W., Zhang, J.Y., Qin, D., Liu, S.H., Li, X.D., Zhang, L.S., 2021. Farnesoid X receptor via Notch1 directs asymmetric cell division of Sox9+ cells to prevent the development of liver cancer in a mouse model. Stem Cell Res. Ther. 12, 232.
Ding, L.X., Lu, S., Zhou, Y., Lyu, D.Y., Ouyang, C.H., Ma, Z.J., Lu, Q.L., 2020. The 3′ untranslated region protects the heart from angiotensin ii-induced cardiac dysfunction via aggf1 expression. Mol. Ther. 28, 1119–1132.
Fernandez-Cantos, M.V., Babu, A.F., Hanhineva, K., Kuipers, O.P., 2024. Identification of metabolites produced by six gut commensal Bacteroidales strains using non-targeted LC-MS/MS metabolite profiling. Microbiol. Res. 283, 127700.
Garibotto, G., Carta, A., Picciotto, D., Viazzi, F., Verzola, D., 2017. Toll-like receptor-4 signaling mediates inflammation and tissue injury in diabetic nephropathy. J. Nephrol. 30, 719–727.
Gan, G.P., Wu, W.Q., Yang, D.S., Yuan, J., 2016. Studies on chemical consitituents of α-glycosidase inhibitory active from rhizome of *Smilax china*. Lishizhen Med. Mater. Medica Res. 27, 2140–2142.
Griffiths, W.J., Koal, T., Wang, Y., Kohl, M., Enot, D.P., Deigner, H.P., 2010. Targeted metabolomics for biomarker discovery. Angew. Chem. Int. Ed. Engl. 49, 5426–5445.
Gurung, M., Li, Z., You, H., Rodrigues, R., Jump, D.B., Morgun, A., Shulzhenko, N., 2020. Role of gut microbiota in type 2 diabetes pathophysiology. EBioMedicine 51, 102590.

Han, F., Zhou, L., Zhao, L., Wang, L., Liu, L., Li, H., Qiu, J., He, J., Liu, N., 2015. Identification of miRNA in sheep intramuscular fat and the role of miR-193a-5p in proliferation and differentiation of 3T3-L1. Front. Genet. 12, 633295.
Hartstra, A, Bouter, V., E, K, Bäckhed, F, Nieuwdorp, M, 2015. Insights into the role of the microbiome in obesity and type 2 diabetes. Diabetes Care 38, 159–165.
He, X.Y., Wang, C.E., Zhu, Y.X., Jiang, X.Q., Qiu, Y.Y., Yin, F., Xiong, W.Y., Liu, B., Huang, Y., 2022. Spirulina compounds show hypoglycemic activity and intestinal flora regulation in type 2 diabetes mellitus mice. Algal. Res. 66, 102791.
Heianza, Y., Sun, D., Bray, G., Qi, L., 2019. Gut microbiota metabolites, amino acid metabolites and improvements in insulin sensitivity and glucose metabolism: the POUNDS lost trial. Gut 68, 263–270.
Hu, Y.B, Liu, X.Y, Zhan, W., 2018. Farnesoid X receptor agonist INT-767 attenuates liver steatosis and inflammation in rat model of nonalcoholic steatohepatitis. Drug Des. Dev. Ther. 12, 2213–2221.
Huang, H., Chen, J., Chen, Y., Xie, J., Xue, P., Ao, T., Chang, X., Hu, X., Yu, Q., 2022. Metabonomics combined with 16S rRNA sequencing to elucidate the hypoglycemic effect of dietary fiber from tea residues. Food Res. Int. 155, 111122.
Huyiligeqi, Dong, X., Yang, C., Xu, G., Cao, S., Fu, J., Lin, L., Ni, J., 2016. Chemical constituents from *Daphne giraldii* nitsche and their contents simultaneous determination by HPLC. eCAM 2016, 9492368.
Jiang, T., Wang, X.X., Scherzer, P., Wilson, P., Tallman, J., Takahashi, H., Li, J., Iwahashi, M., Sutherland, E., Arend, L., Levi, M., 2007. Farnesoid X receptor modulates renal lipid metabolism, fibrosis, and diabetic nephropathy. Diabetes 56, 2485–2493.
Jiang, C., Xie, C., Lv, Y., Li, J., Krausz, K.W., Shi, J., Brocker, C.N., Desai, D., Amin, S.G., Bisson, W.H., Liu, Y., Gavrilova, O., Patterson, A.D., Gonzalez, F.J., 2015. Intestine-selective farnesoid X receptor inhibition improves obesity-related metabolic dysfunction. Nat. Commun. 6, 10166.
Jiang, X.C., Paultre, F., Pearson, T.A., Reed, R.G., Francis, C.K., Lin, M., Berglund, L., Tall, A.R., 2000. Plasma sphingomyelin level as a risk factor for coronary artery disease. Arterioscler. Thromb. Vasc. Biol. 20, 2614–2618.
Kern, M., Klöting, N., Mark, M., Mayoux, E., Klein, T., Blüher, M., 2016. The SGLT2 inhibitor empagliflozin improves insulin sensitivity in db/db mice both as monotherapy and in combination with linagliptin. Metabolism 65, 114–123.
Li, W., Li, L., Yang, F., Hu, Q., Xiong, D., 2022. Correlation between gut bacteria Phascolarctobacterium and exogenous metabolite α-linolenic acid in T2DM: a case-control study. Ann. Transl. Med. 10, 1056.
Li, X., Yang, L, C, Xu, M, Qiao, G, X., Li, C.J., Lin, L.Z., Zheng, G.D., 2021. *Smilax china* L. polyphenols alleviates obesity and inflammation by modulating gut microbiota in high fat/high sucrose diet-fed C57BL/6J mice. J. Funct. Foods 77, 104332.
Liu, Z., Dai, X., Zhang, H., Shi, R., Hui, Y., Jin, X., Zhang, W., Wang, L., Wang, Q., Wang, D., Wang, J., Tan, X., Ren, B., Liu, X., Zhao, T., Wang, J., Pan, J., Yuan, T., Chu, C., Lan, L., Liu, X., 2020. Gut microbiota mediates intermittent-fasting alleviation of diabetes-induced cognitive impairment. Nat. Commun. 11, 1–14.
Ma, S.P., Wei, M., Guo, J., Zhao, L.M., Wei, M, 1998. Effects of Rhizoma Smilacinus on blood glucose level and hepatic glycogen in mice. Chin. J. Mod. Appl. Pharm. 5, 5–7.
Malik, M.A., Raza, M.K., Dar, O.A., Amadudin, Abid.M., Wani, M.Y., Al-Bogami, A.S., Hashmi, A.A., 2019. Probing the antibacterial and anticancer potential of tryptamine based mixed ligand Schiff base Ruthenium(III) complexes. Bioorg. Chem. 87, 773–782.
Newman, D.J., Cragg, G, M, 2012. Natural products as sources of new drugs over the 30 years from 1981 to 2010. J. Nat. Prod. 75, 311–335.
Qin, L., Zhang, X., Zhou, X., Wu, X., Huang, X., Chen, M., Wu, Y., Lu, S., Zhang, H., Xu, X., Wei, X., Zhang, S., Huang, R., 2020. Protective effect of benzoquinone isolated from the roots of *Averrhoa carambola* L. on streptozotocin-induced diabetic mice by inhibiting the TLR4/NF-κB signaling pathway. Diabetes Metab. Syndr. Obes. 13, 2129–2138.
Rodriguez-Diaz, C., Taminiau, B., García-García, A., Cueto, A., Robles-Díaz, M., Ortega-Alonso, A., Martín-Reyes, F., Daube, G., Sanabria-Cabrera, J., Jimenez-Perez, M., Isabel Lucena, M., Andrade, R.J., García-Fuentes, E., García-Cortes, M., 2022. Microbiota diversity in nonalcoholic fatty liver disease and in drug-induced liver injury. Pharmacol. Res. 182, 106348.
Schlitt, A., Blankenberg, S., Yan, D., von Gizycki, H., Buerke, M., Werdan, K., Bickel, C., Lackner, K.J., Meyer, J., Rupprecht, H.J., Jiang, X.C., 2006. Further evaluation of plasma sphingomyelin levels as a risk factor for coronary artery disease. Nutr. Metab. (Lond.) 3, 5.
Shang, L., Li, F., Zhu, J., Sun, C., Wang, Y., 2023. Selenium-Enriched and ordinary black teas regulate the metabolism of glucose and lipid and intestinal flora of hyperglycemic mice. Plant Foods Hum. Nutr. 78 (1), 61–67.
Somm, E., Montandon, S.A., Loizides-Mangold, U., Gaïa, N., Lazarevic, V., De Vito, C., Perroud, E., Bochaton-Piallat, M.L., Dibner, C., Schrenzel, J., Jornayvaz, F.R., 2021. The GLP-1R agonist liraglutide limits hepatic lipotoxicity and inflammatory response in mice fed a methionine-choline deficient diet. Transl. Res. 227, 75–88.
Shiragannavar, V.D., Sannappa Gowda, N.G., Puttahanumantharayappa, L.D., Karunakara, S.H., Bhat, S., Prasad, S.K., Kumar, D.P., Santhekadur, P.K., 2023. The ameliorating effect of withaferin A on high-fat diet-induced non-alcoholic fatty liver disease by acting as an LXR/FXR dual receptor activator. Front. Pharmacol. 14, 1135952.
Thangam, E.B., Jemima, E.A., Singh, H., Baig, M.S., Khan, M., Mathias, C.B., Church, M. K., Saluja, R., 2018. The role of histamine and histamine receptors in mast cell mediated allergy and inflammation: the hunt for new therapeutic targets. Front. Immunol. 9, 1873.
Tett, A., Pasolli, E., Masetti, G., Ercolini, D., Segata, N., 2021. Prevotella diversity, niches and interactions with the human host. Nat. Rev. Microbiol. 19, 585–599.
Valencia-Ortega, J., González-Reynoso, R., Salcedo-Vargas, M., Díaz-Velázquez, M.F., Ramos-Martínez, E., Ferreira-Hermosillo, A., Mercado, M., Saucedo, R., 2023. Differential expression of fxr and genes involved in inflammation and lipid metabolism indicate adipose tissue dysfunction in gestational diabetes. Arch. Med. Res. 54 (3), 189–196.
Wang, C, Zhao, S, Xu, Y, Sun, W, Feng, Y, Liang, D, Guan, Y., 2022. Integrated microbiome and metabolome analysis reveals correlations between gut microbiota components and metabolic profiles in mice with methotrexate-induced hepatoxicity. Drug Des. Dev. Ther. 16, 3877–3891.
Wang, Z., Klipfell, E., Bennett, B.J., Koeth, R., Levison, B.S., Dugar, B., Feldstein, A.E., Britt, E.B., Fu, X., Chung, Y.M., Wu, Y., Schauer, P., Smith, J.D., Allayee, H., Tang, W.H., DiDonato, J.A., Lusis, A.J., Hazen, S.L., 2011. Gut flora metabolism of phosphatidylcholine promotes cardiovascular disease. Nature 472, 57–63.
Wang, H., Shen, Q., Zhang, F., Fu, Y., Zhu, Y., Zhao, L., Wang, C., Zhao, Q., 2023. Heat-treated foxtail millet protein delayed the development of pre-diabetes to diabetes in mice by altering gut microbiota and metabolomic profiles. Food Funct. 14, 4866–4880.
Wang, Z., Chen, W.H., Li, S.X., He, Z.M., Zhu, W.L., Ji, Y.B., Wang, Z., Zhu, X.M., Yuan, K., Bao, Y.P., Shi, L., Meng, S.Q., Xue, Y.X., Xie, W., Shi, J., Yan, W., Wei, H., Lu, L., Han, Y., 2021. Gut microbiota modulates the inflammatory response and cognitive impairment induced by sleep deprivation. Mol. Psychiatry 26, 6277–6292.
Xue, C., Li, G.L., Zheng, Q.X., Gu, X.Y., Shi, Q.M., Su, Y.S., Chu, Q.F., Yuan, X., Bao, Z.Y., Lu, J., Li, L.J, 2023. Tryptophan metabolism in health and disease. Cell Metab. 35, 1304–1326.
Yan, X., Zhang, Y., Peng, Y., Li, X., 2022. The water extract of Radix scutellariae, its total flavonoids and baicalin inhibited CYP7A1 expression, improved bile acid, and glycolipid metabolism in T2DM mice. J. Ethnopharmacol. 293, 115238.
Yang, W., Xia, Z., Zhu, Y., Tang, H., Xu, H., Hu, X., Lin, C., Jiang, T., He, P., Shen, J., 2023. Comprehensive study of untargeted metabolomics and 16S rRNA reveals the mechanism of fecal microbiota transplantation in improving a mouse model of T2D. Diabetes Metab. Syndr. Obes. 16, 1367–1381.
Yano, J.M., Yu, K., Donaldson, G.P., Shastri, G.G., Ann, P., Ma, L., Nagler, C.R., Ismagilov, R.F., Mazmanian, S.K., Hsiao, E.Y., 2015. Indigenous bacteria from the gut microbiota regulate host serotonin biosynthesis. Cell 161, 264–276.
Yang, L., Zhao, Y., Pan, Y., Li, D., Zheng, G., 2019. Dietary supplement of *Smilax china* L. ethanol extract alleviates the lipid accumulation by activating AMPK pathways in high-fat diet fed mice. Nutr. Metab. 16, 6–17.
Yin, W., Zhang, S.Q., Pang, W.L., Chen, X.J., Wen, J., Hou, J., Wang, C., Song, L.Y., Qiu, Z.M., Liang, P.T., Yuan, J.L., Yang, Z.S., Bian, Y., 2022. Tang-Ping-San decoction remodel intestinal flora and barrier to ameliorate type 2 diabetes mellitus in rodent model. Diabetes Metab. Syndr. Obes. 15, 2563–2581.
Yudhani, R.D., Sari, Y., Nugrahaningsih, DAA., Sholikhah, E.N., Rochmanti, M., Purba, AKR., Khotimah, H., Nugrahenny, D., Mustofa, M., 2023. In vitro insulin resistance model: a recent update. J. Obes. 2023, 1964732.
Zhang, D.D., Li, H.J., Luo, X.Y, Liu, D., Wei, Q., Ye, X.C., 2022a. Integrated 16S rDNA, metabolomics, and TNF-α/NF-κB signaling pathway analyses to explain the modulatory effect of *Poria cocos* aqueous extract on anxiety-like behavior. Phytomedicine 104, 154300.
Zhang, J., Wang, W., Guo, D., Bai, B., Bo, T., Fan, S., 2022b. Antidiabetic effect of millet bran polysaccharides partially mediated via changes in gut microbiome. Foods. 11, 3406.
Zhang, X.L., Yan, Y.H., Zhang, F., Zhang, X.R., Xu, H., Liu, Y., Huang, Y.H., 2023. Analysis of the effect of hyaluronic acid on intestinal flora and its metabolites in diabetic mice via high-throughput sequencing and nontargeted metabolomics. J. Funct. Foods 103, 105496.
Zhou, W., Han, L., Haidar Abbas Raza, S., Yue, Q., Sun, S., Zhao, Y., Lv, L., Deng, Y., Yuan, Z., Alsharif, I., Mohammedsaleh, Z.M., Alaryani, F.S., Alhumaidi Alotaibi, M., Albiheyri, R.S., Al-Sarraj, F.M., Hasan Mukhtar, M., 2023. Polysaccharides in *Berberis dasystachya* improve intestinal flora depending on the molecular weight and ameliorate type 2 diabetes in rats. J. Funct. Foods 100, 105381.
Liao, J., Cao, Y., Zhao, J., Yu, B., Wang, Y., Li, W., Li, H., Lv, S., Wen, W., Cui, H., Chen, Y., 2023. Aqueous extract of *Polygala japonica* Houtt. ameliorated nonalcoholic steatohepatitis in mice through restoring the gut microbiota disorders and affecting the metabolites in feces and liver. Phytomedicine 118, 154937.